

## Update of the ESA Space Debris Mitigation Handbook

### Executive Summary

**ESA Contract 14471/00/D/HK**

**July 2002**

**Ref: QINETIQ/KI/SPACE/CR021539**

Authors:

R. Walker            QinetiQ Ltd., Cody Technology Park, Farnborough, Hants., U.K.  
C. Martin  
H. Stokes  
J. Wilkinson

H. Sdunnus        eta\_max space GmbH, Richard Wagner Str., Braunschweig, Germany  
S. Hauptmann  
P. Beltrami

H. Klinkrad        European Space Operations Centre, Robert Bosch Str., Darmstadt, Germany

ESA Study Manager: H. Klinkrad

**The work described in this report was done under ESA contract.  
Responsibility for the contents resides in the authors or organisations  
that prepared it.**

# CONTENTS

---

## **1 Summary of the Handbook Content**

- 1.0 Overview
- 1.1 Introduction
- 1.2 The current orbital debris and meteoroid environments
- 1.3 Impact flux analysis for space vehicle design
- 1.4 The future space debris environment
- 1.5 Long-term effectiveness of debris mitigation measures
- 1.6 Long-term forecasting of debris impact risk
- 1.7 Debris mitigation guidelines and techniques
- 1.8 Post-mission disposal assessment
- 1.9 Re-entry survivability and on-ground risk assessment
- 1.10 On-Orbit collision avoidance assessment
- 1.11 Spacecraft protection

## **2 The Handbook Web Environment**

- 2.0 The Handbook Web Environment

## **3 Conclusions**

- 3.0 Summary and Conclusions

## **Glossary**

# 1

---

## SUMMARY OF THE HANDBOOK CONTENT

## 1.0 Overview

The ESA Space Debris Mitigation Handbook intends to provide technical support to projects in the following areas:

- description of the current space debris and meteoroid environment
- assessment of risk potentials due to debris and meteoroid impacts
- analysis of the future space debris environment
- implementation of efficient space debris mitigation measures
- assessment of risk due to re-entries
- planning of debris shielding and/or collision avoidance concepts matching the mission needs and system capabilities

The ESA Space Debris Mitigation Handbook together with the European Space Debris Mitigation and Safety Standard shall jointly define the Agency's policies and implementation concepts concerning space debris mitigation and collision risk reduction for any mission under ESA control.

The handbook chapters are summarised in the following sections.

## 1.1 Introduction

Nominal space operations and on-orbit fragmentations have created a large number of man made space debris. Together with natural objects (meteoroids) they contribute to the Earth particulate environment. As of 31 Dec 1997, 3,896 launches had resulted in 25,130 objects which were tracked and registered by the United States Space Command (USSPACECOM). The corresponding catalogue of on-orbit objects at this epoch had 8,325 entries, of which about 43% had their origin in one of the 144 fragmentation events up to Dec. 1997. The USSPACECOM catalogue covers trackable objects larger than about 10 cm in LEO and objects larger than about 1 m in GEO. The small-size, uncatalogued population as modelled by the ESA MASTER Model consists of more than 360,000 objects larger than 1 cm, about  $1.8 \cdot 10^8$  objects larger than 1 mm, and more than  $1.2 \cdot 10^{11}$  objects larger than 0.1 mm. In the smaller size regime, paint flakes, residues from solid rocket motor firings, and ejecta are known to contribute to the debris population. Presently, the man-made debris environment in most LEO regions is assumed to dominate the natural meteoroid contribution, except for a confined size regime around 0.1 mm diameters.

The current debris population poses a certain collision probability and a resulting risk of damage to orbiting objects which are exposed to this environment. The collision probability can be assessed by applying debris flux models for size regimes and for certain target orbits of interest. In general, the current risk from debris is not yet unacceptably high for a single target object. The current collision probability among all objects larger than 1 cm is about 7% per year. However, for some operational spacecraft, and particularly for manned missions where tolerable risk levels are low, protective measures may be necessary to enable safe operations in the given particulate environment, and to reduce the consequences of the impacts of smaller objects.

If one assumes certain scenarios for future space flight activities, 'business as usual' practices are expected to lead to an onset of interactive collisions among larger, catalogued objects. Thus, fragments from collisions, to date an insignificant source of space debris, will grow to dominate the man made debris population larger than 1 cm in diameter. Finally, once a so called 'critical object density' is reached at some altitudes, a process of collisional cascading may set in (collisional fragments will trigger further collisions). The resulting growth will be non-linear. But even before such a process starts, the debris population will grow and, due to the increasing number of objects, the collision risk in space for active spacecraft will grow correspondingly.

The uncontrolled growth of the space debris population has to be avoided in order to enable safe operations in space for the future. Computer simulations can be used to demonstrate the suitability of different levels of mitigation measures to limit and control the future growth of the space debris population. The common goal of these measures is to reduce the number of future objects released into space to the maximum possible extent. This can be done directly (e.g. by reducing mission related objects), or indirectly (e.g. by passivating upper stages to avoid subsequent explosions). The implementation of passivation measures at end of mission would reduce the debris contributions from on-orbit explosions – the dominant historic debris source – at the cost of technical modifications of the spacecraft or upper stages. Ultimately, however, only the removal of large cross-sections and masses from orbit (e.g. de-orbit of spacecraft and upper stages at end-of-mission) can suppress collisions as the dominating source of debris in the future. Computer simulations with the ESA DELTA model have shown that this objective would be achieved by the reduction of orbital lifetimes of massive objects in LEO to 25 years. This limitation on the orbital lifetime has been found to be a good compromise between benefit to the space environment, collision risk reduction, manoeuvre requirements and responsiveness to significant increases in launch traffic. In exceptional cases, where lifetime reduction and de-orbiting is not practicable, the manoeuvring of a spacecraft to a disposal orbit (e.g. above LEO or GEO) will be required at the end of the mission operations.

## 1.2 The current orbital debris and meteoroid environments

This chapter describes the current situation of the space debris environment explaining how space debris is created and what sources produce it. The data presented in this chapter was mainly obtained from the Database and Information System Characterising Objects in Space (DISCOS) [1] and from the MASTER'99 debris and meteoroid model [2], [3].

Since the beginning of spaceflight in the 1950's a total of 27,061 objects (as of 31.01.2002) have been released into orbits around Earth. The continually growing space activity and various debris generation mechanisms related to them (e.g. 170 on-orbit fragmentation events until 05 September 2001) have resulted in a continuous growth of the space debris population. The following sections describe the different sources of space debris.

### Launch history

Most of the data on space debris is collected by the United States Space Command (USSPACECOM) using its Space Surveillance Network (SSN). This network of electro-optical and radar sensors detects, tracks and identifies Earth orbiting objects in a catalogue. The USSPACECOM catalogue contains data of objects larger than about 10 cm to 30 cm in LEO, and objects larger than about 1 m in GEO, i.e. rocket bodies, payloads, and larger debris objects. Up to October 2001, a total of 4643 launches had been recorded and the number of unclassified catalogue objects on orbit was 8,993, which is about one third of the total count of 27061 objects which had entered the catalogue to date. The remaining two thirds of the objects had re-entered the Earth atmosphere in an uncontrolled manner (due to natural decay), or controlled manner (due to de-orbit). Fig. 1.2-1 shows the current number of on-orbit catalogued objects versus time for payloads and debris.

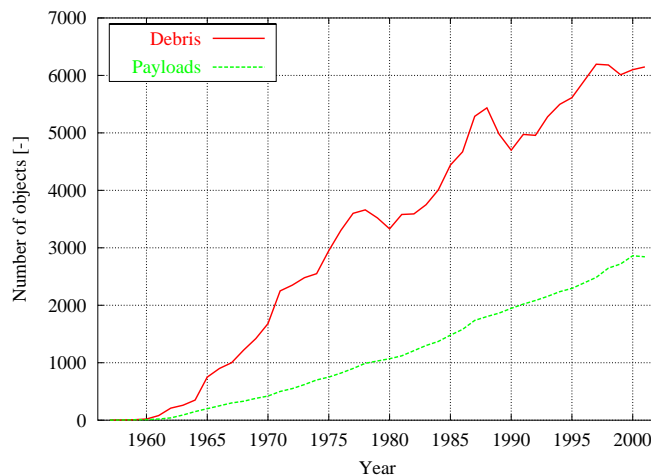


Figure 1.2-1: History of the on-orbit catalogue population as a function of time

On 5 September 2001, the catalogue population consisted of 30.6% operational and non-operational payloads (= 2,567), 16.7% rocket bodies (= 1,400), 9.8% operational debris (= 821) and 42.9% payload and rocket debris (= 3,595). Only about 6% of the catalogue population can be assumed to be operational payloads.

### Historic fragmentation events

Fragmentations are a major source of the current population of debris objects larger than about 1 cm. In total, 170 fragmentations have been recorded up to 30 May 2001 [4]. The major causes of known breakups between 1961 and May 2001 are summarized in Tab. 1.2-1.

cause	events
unknown	56
aerodynamic	9
deliberate explosion	48
propulsion related	49
electrical	7
collision	1
total	170

Table 1.2–1: *Causes of the historical breakups as of 30 May 2001 (note that one event flagged as ‘deliberate’ was related to a collision).*

The primary causes of satellite breakups are deliberate actions and propulsion-related events, although the cause for about one in three breakups remains uncertain. Currently, propulsion-related breakups are the most frequent class.

### Non-fragmentation debris sources

In-situ impact measurements by on-orbit detectors and from post-flight analysis of returned surfaces (e.g. LDEF, EURECA, HST) give evidence of non-fragmentation sources, mainly in the sub-mm size regime, contributing to the man-made debris environment. However, very little information on the particulate environment for Earth orbits above about 600 km altitude is available. Especially, the space debris environment in the important geostationary ring is largely unknown. The mechanisms related to the generation of small debris particles are still not well understood for most source terms. Non-fragmentation sources generating objects up to centimetre sizes and beyond have been correlated with solid rocket motor dust and slag, sodium-potassium (NaK) reactor coolant liquids, ejecta particles, paint flakes and with clusters of dipoles which formed after the “Westford Needles” release experiment in 1963.

### The orbital debris environment

In this section the number of objects and the spatial density in the current orbital debris environment as modelled in the MASTER’99 debris and meteoroids model is described. The MASTER’99 model [3], [5], [6] covers all orbital regions from LEO up to GEO and has a lower size threshold of 1  $\mu\text{m}$ . It describes the man-made and natural particulate environment of the Earth and its incident flux on user-defined target orbits.

The mean numbers of objects of the LEO, MEO and GEO debris environment according to the ESA MASTER’99 model are given in table 1.2–2. The object numbers are weighted by the relevant resident times in LEO. Hence, objects on highly elliptical orbits contribute only with a certain fraction.

debris size	objects in LEO	objects in MEO	objects in GEO
> 0.1 mm	$1.03 \cdot 10^{10}$	$1.6 \cdot 10^{11}$	$2.5 \cdot 10^{10}$
> 1 mm	$3.8 \cdot 10^7$	$1.6 \cdot 10^8$	$2.1 \cdot 10^7$
> 1 cm	121,289	173,244	20,703
> 10 cm	13,207	2,191	564

Table 1.2–2: *Space debris population breakdown with size according to the ESA MASTER’99 model*

Figure 1.2–2 shows that, in the LEO environment, peak concentrations are most pronounced for objects larger than 1 cm and for catalogue objects (> 10 cm). The peak in the LEO semi-major axis distribution around  $a = 7,300$  km relates to mostly near-circular orbits in the densely populated

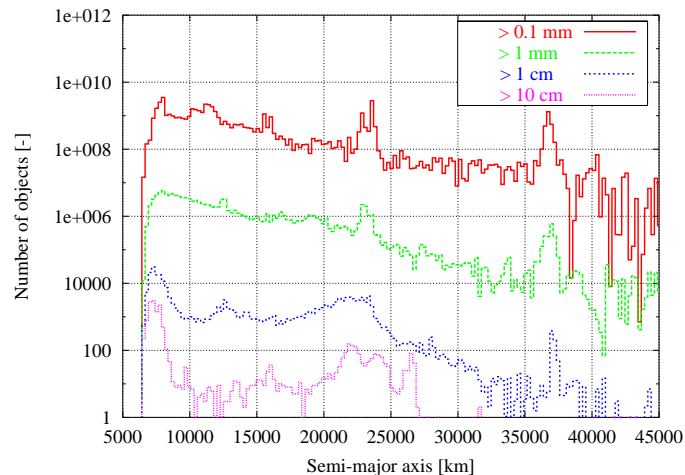


Figure 1.2-2: Number of debris objects in the LEO environment as a function of semi-major axis according to MASTER'99 (class width 243.5 km)

altitude region around 1,000 km. The maximum at  $a = 24,400$  km is due to GTO-type 10.5 h orbits while the neighbouring peak at  $a = 27,000$  km corresponds to LEO passes of highly eccentric Molniya-type 12 h orbits. The peak at 37000 km for  $d > 0.1$  mm,  $d > 1$  mm and  $d > 1$  cm are mainly produced by the SRM firings of the inertial upper stages of Shuttle missions STS-93 and STS-33R into GTO/HEO orbits.

In the MEO region, peak concentrations are most pronounced for catalogue objects ( $> 10$  cm) with a maximum around  $a = 27,000$  km relating to the 12 h orbits (e.g. Molniya, GPS, GLONASS) and the GTO transfer orbits of 10.5 h. A larger peak at 42,000 km is caused by 24 h orbit periods, e.g. Tundra or near-GEO missions. For smaller objects the distributions become more uniform. Here, peaks produced by the firings of solid rocket motors in near GEO-orbits are located at 40,000 km and at about 27,000 km. The GEO semimajor axis distribution shows an increased number of objects around  $a = 25,000$  km and 27,000 km related to 10.5 h GTO transfer trajectories and to 12 h orbits (e.g. Molniya satellites). A peak prevails at 42,000 km corresponding to 24 h orbit periods of GEO and near-GEO objects. Objects smaller than 10 cm have a peak somewhat below GEO at around 40,000 km produced by the large number of solid rocket motor firings of apogee kick motors.

In all orbit regions near-circular orbits dominate, followed by a large number of objects in highly eccentric GTO and Molniya orbits. Small particles also show large numbers of circular and GTO orbits, but have a much more uniform distribution of the eccentricity.

The distribution of articulated inclination bands for LEO and MEO can be correlated with major launch site latitudes (e.g. Korou at  $i = 7$  deg, KSC at  $i = 28.5$  deg, Tyuratam at  $i = 45.6$  deg, Plesetsk at  $i = 62.8$  deg), and with certain mission objectives (e.g. polar orbits at  $i = 90$  deg, sun-synchronous orbits at around  $i = 100$  deg). The inclination distribution of the GEO population is governed by near-GEO objects on near-circular orbits which are kept within a deadband of  $i \in (0, 15^\circ)$  due to a 54 year cyclic perturbation.

The distribution of the spatial density in LEO is plotted in fig. 1.2-3 as a function of altitude and declination. The plot is based on the ESA MASTER'99 model for objects  $> 1$  cm. In LEO, high object concentrations are noticeable at latitudes corresponding to declinations of  $\delta = \pm i_{max}$ , where  $i_{max}$  denotes densely populated inclination bands at about  $65^\circ$ , and at altitudes bands around 900–1,000 km and around 1,500 km. The MEO distribution of the spatial density presents high object concentrations at altitudes bands around 20,000 km (12 h orbits), 35,800 km (24 h orbits), and close to LEO. The spatial density in GEO shows a clear concentration of objects at 35,786 km with very low inclinations, especially for objects  $> 1$  cm.



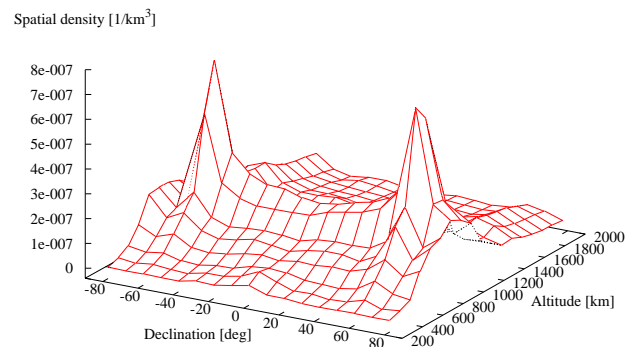


Figure 1.2–3: The spatial density in LEO as a function of declination and altitude according to MASTER'99 for  $d > 1$  cm (class width 10 deg for declination and 100 km for altitude)

## Meteoroid environment

Meteoroids are particles in space which are of natural origin. Nearly all meteoroids originate from comets and asteroids. The natural meteoroid environment represents, at any instant, a total mass of about 200 kg within 2000 km altitude from the Earth's surface.

Random meteoroid fluxes with no apparent time correlation are called 'sporadic' contributions. They account for about 90 % of the annual mean flux level. Meteoroids which retain the orbit of their parent body can create annually recurring events of concentrated flux peaks with well defined directional and velocity properties. They are called 'streams'. The total time averaged meteoroid environment (annual average of sporadics plus streams) is called 'background' meteoroids.

The mass density of meteoroids varies widely from about  $0.15 \text{ g/cm}^3$  to  $8 \text{ g/cm}^3$ . According to [7] the average density of micro-meteoroids larger than  $0.01 \text{ g}$  is assumed to be  $0.5 \text{ g/cm}^3$ . Meteoroids smaller than  $10^{-6} \text{ g}$  are thought to have a higher mean density of  $2 \text{ g/cm}^3$ . The recommended value for masses between  $10^{-6} \text{ g}$  and  $0.01 \text{ g}$  is  $1 \text{ g/cm}^3$ . There is, however, a considerable uncertainty associated with these densities.

### 1.3 Impact flux analysis for space vehicle design

The Handbook chapter “Impact flux analysis for space vehicle design” describes the space debris and meteoroid impact flux (in impacts per m<sup>2</sup> and year) as modelled by the MASTER’99 space debris model for spacecraft in different orbits. This chapter includes 2-D and 3-D plots showing the flux levels versus a large number of orbital parameters for four types of orbit (LEO, GTO, MEO and GEO). The large number of figures produced were generated automatically using the MADESC tool developed by eta.max space. MADESC is a Perl script capable of automatically running MASTER’99 for a large number of target orbits. Tables can be generated with for flux results versus all relevant orbital parameters.

MADESC produces 2-D plots from these flux tables using the Gnuplot graphic tool. 3-D plots can also be produced using tables of flux versus any two parameters relating to impact velocity and direction. Figure 1.3–1 schematically shows the tasks performed by the MADESC tool.

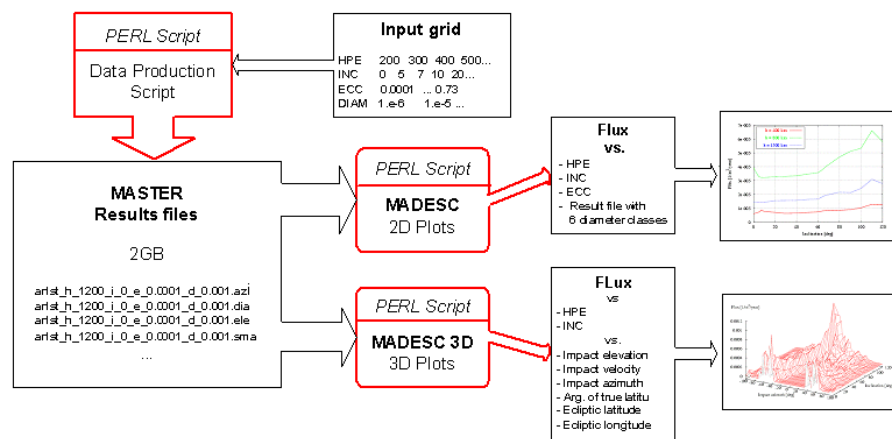


Figure 1.3–1: MASTER Data Extraction Script

The mean times between debris impacts on a target satellite in LEO is listed in Table 1.3–1 as a function of the impactor size, for a given mean orbital altitude of the target. The table provides results averaged over all possible target orbit inclinations between 0 and 120 degrees as well as minimum, maximum and mean values for the relevant altitudes. The cross sectional area of the target is assumed to be 100 m<sup>2</sup>.

#### Impact flux from space debris on LEO missions

Figure 1.3–2 shows the distribution of the debris flux over perigee altitude for orbits with various orbit inclinations for sizes larger than 1 mm. Retrograde orbits with high inclinations around 100 deg show the highest impact fluxes. The highest impact rates can be seen at altitudes between 750 km and 1,000 km. The plots show a more equal distribution above 1000 km. Orbits with inclinations around  $i = 110$  deg show the highest fluxes due to densely populated complementary inclination bands at  $i = 82$  deg, 75 deg, and 65 deg, which yield high relative velocities (i.e. high sampling rates) due to near head-on collision geometries. Figure 1.3–3 shows the collision flux distribution in terms of the azimuth angle  $A$  as a function of target orbit inclination for 800 km altitude. Due to the changing signature of the densely populated debris inclination bands with target inclination, there are peak fluxes from  $A = \pm 60$  deg for low inclinations (with almost no contributions from a sector within  $A = \pm 30$  deg, due to the lack of retrograde debris), while the two flux peaks merge for high, retrograde inclinations.

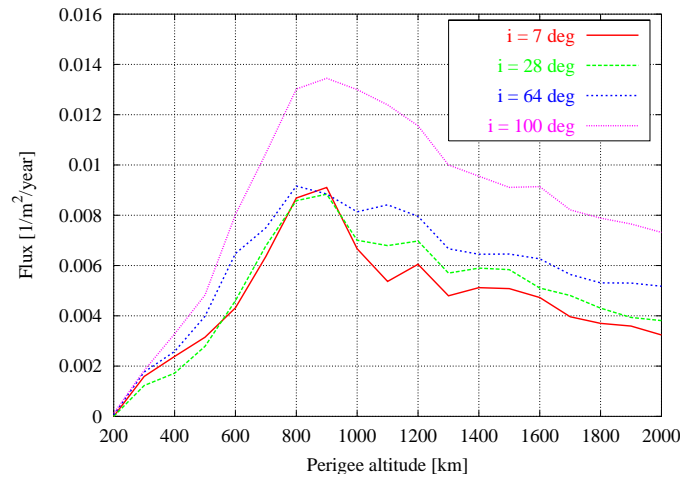


Figure 1.3–2: LEO collision flux from debris as a function of altitude of the target orbit for  $d > 1$  mm.

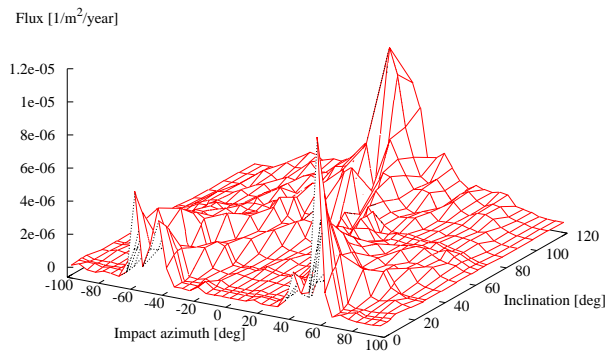


Figure 1.3–3: LEO distribution of debris flux as a function of impact azimuth and inclination for a near-circular target orbit at 800 km for  $d > 1$  cm

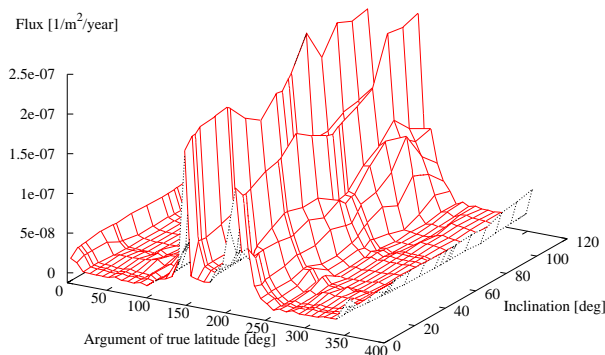


Figure 1.3–4: Distribution of debris flux as a function of argument of true latitude and inclination for a GTO-type target orbit with 400 km perigee altitude for  $d > 1$  cm

altitude	Time between impacts from debris objects larger than				
		0.1 mm	1 mm	1 cm	10 cm
400 km	mean	4.5 d	3.9 y	1,214 y	16,392 y
	max	1.3 d	2.2 y	776 y	10,813 y
	min	33.1 d	5.9 y	1,674 y	21,853 y
800 km	mean	2.3 d	1.0 y	245 y	1,775 y
	max	1.3 d	0.6 y	151 y	1,198 y
	min	3.4 d	1.2 y	310 y	2,329 y
1,500 km	mean	0.9 d	1.5 y	534 y	3,109 y
	max	0.6 d	0.8 y	323 y	2,058 y
	min	1.4 d	2.0 y	698 y	4,305 y

Table 1.3–1: Mean, maximum and minimum time between debris impacts on a target object of 100 m<sup>2</sup> cross sectional area as a function of impactor size and orbital altitude (results according to the MASTER '99 model)

### Impacts from space debris on GTO and HEO orbits

For GTO and HEO orbits, largest collision fluxes are encountered on high inclination orbits due to the dominance of small-size fragments which originate from fragmentation events in the 65 deg inclination band and above. A considerable peak can be seen around 28 deg corresponding to breakup events and solid rocket motor firing events related to launches from KSC. The temporal variation of flux magnitude along the target orbit is illustrated in fig. 1.3–4 as a function of the argument of true latitude  $u$  of the orbit. Almost independent from target orbit inclination the flux maxima occur around perigee passes through the high spatial densities in LEO (at  $u \approx 150$  deg and 210 deg), with another sub-peak for locations of GEO transits (at  $u \approx 0$  deg).

### Impact flux from space debris on MEO missions

In MEO, the flux level is higher at those altitudes with high spatial densities near LEO, and it shows a peak at 20,000 km altitude corresponding to the higher density produced by navigation satellite constellations. Large fluxes originate from inclinations around 28 deg due to large concentrations of SRM particles of cm sizes and below. Large collision fluxes are also produced from explosion fragments on high inclination orbits at  $i = 65^\circ$  and above. The elevation distribution of debris flux  $> 10$  cm on a near-circular GPS-type orbit in fig. 1.3–5 shows two symmetric peaks at about  $h \approx \pm 60$  deg elevation which move to  $h \approx \pm 20$  deg elevation with higher inclinations. This is the angle under which HEO fragment orbits intersect GPS-type targets in their altitude band during earthbound and spacebound transits. The peak at 0 deg elevation increases with target orbit inclination due to higher spatial densities at high latitudes.

### Impact flux from space debris on GEO missions

In GEO, the largest collision fluxes are encountered on low inclination orbits due to the concentration of operational payloads near  $i \approx 0$  deg, and due to the trapping of defunct payloads and mission related objects within an inclination band of 0 deg and 15 deg ( $\pm 7.5$  deg with respect to the stable Laplace plane at  $i = 7.5$  deg). Most impacts in GEO have low impact velocities due to most of the debris having low velocities and low inclination orbits. Collisions with slow HEO and GTO objects near their apogee increase the impact velocity to around 1.5 km/s for higher inclination orbits. For catalog-size debris, low velocity "rendez-vous" type collisions at azimuth  $A \approx \pm 90$  deg are prevailing in GEO with impact velocities less than 800 m/s, while near head-on collisions at high relative velocities are in the minority for objects larger than 1 cm.

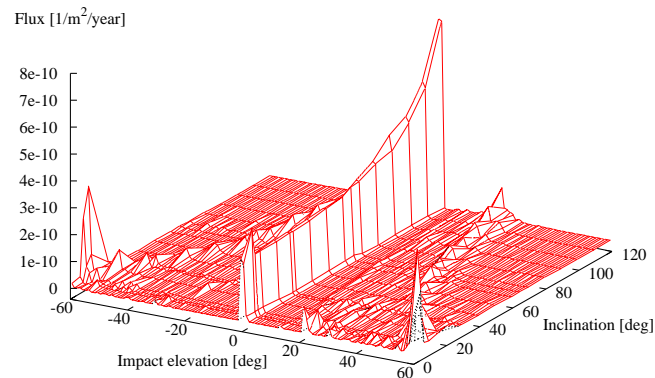


Figure 1.3–5: MEO distribution of debris flux as a function of impact elevation and target inclination for a MEO near circular orbit at 20,000 km for  $d > 10$  cm

### Impact flux from meteoroids

The impact risk posed by meteoroids depends only slightly on the characteristics of a terrestrial target orbit (in contrast with the space debris flux), due to a relatively homogeneous spatial density of meteoroids in the Earth environment. Gravitational focussing effects of the Earth (increasing the flux), and geometrical shielding of a certain part of the celestial sphere by the Earth (decreasing the flux) lead to altitude and position dependent flux modulations.

The influence of the target orbit inclination on the meteoroid flux is much less than for debris due to the higher velocities of meteoroid particles. Targets in LEO are the only ones slightly affected by the orbit inclination due to their relatively high orbit velocities. The impact velocity for meteoroids ranges from 10 and 72 km/s, three to four times higher than for debris. The effect of Earth shielding on meteoroid flux becomes evident from the blocking of flux directions at elevations  $h < 0$  deg on orbits at low altitudes. The effect of gravitational focussing is noted by higher peak fluxes, and by corresponding increases in the mean collision velocity for LEO orbits.

In addition to the background meteoroids, meteoroid streams contribute about 10% of the annual mean meteoroid flux, generating sharp, time-limited flux peaks as the Earth crosses the trails of periodic comet orbits. The flux directions and peak times can be predicted quite accurately, while the flux levels are less well defined.

## 1.4 The future space debris environment

Before determining the most effective measures that should be taken to solve the space debris problem in Earth orbit, it is essential to quantify the problem not only in terms of the current orbital debris environment, but also its future growth potential without remedial action. As a result of continuing growth, the orbital debris population will reach a critical level, where random collisions will start to occur and produce even more fragments. When the rate of fragments being produced by random collisions exceeds the rate at which they are being removed by atmospheric drag, the debris population will start to grow exponentially as collision fragments cause more collisions, and so on. This is a process called collision cascading [8] or chain reaction [9]. It is this potential dominance of uncontrollable random collisions over controllable explosions as the main source of debris that has prompted the need to establish international debris mitigation practices.

The ESA DELTA (Debris Environment Long Term Analysis) model is used to provide predictions of the long-term evolution of the orbital debris environment and associated collision risks in the handbook. DELTA utilises the MASTER-99 reference population as its starting point for the long-term projections. In all, some 25 studies were performed with DELTA: 19 studies dealing only with LEO, and 6 studies considering a full LEO/MEO/GEO simulation. Due to the fact that DELTA is a Monte Carlo simulation, each study needs 10 runs of different random conditions in order to obtain a reasonable average in the model output. This simulation process resulted in over 4100 hours of CPU time consumption and over 200 Gb of output data storage. Overall, 68 plots were generated for the handbook using DELTA results, and many more extra plots were created for the Handbook Web Environment.

This chapter presents the potential extent of the space debris problem in Earth orbit over the next century, should mankind neglect to take steps soon in order to solve this problem. This is defined by the 'Business As Usual' scenario whereby no mitigation measures are implemented and recent space traffic continues at the same average, constant rate into the long-term future. A full breakdown of debris source population contributions is given for Business As Usual evolution in the LEO and GEO regions, including spatial density as a function of altitude. Long-term predictions of total LEO, MEO and GEO population levels are also compared for different debris size thresholds (1 mm, 1 cm, 10 cm, 1 m). The predicted evolution of collision activity in LEO is presented as a function of orbital altitude and inclination.

If there were no debris mitigation measures implemented in the future and spaceflight activity continued according to the recent past, then we might expect that the large object population would continue to grow in an overall linear manner over the next century (Figure 1.4–1). This would be caused by the accumulation of launch/mission-related objects and fragments from explosions. However, such growth would be sufficient to produce an increasing rate of collisions between these large objects in the LEO region over the next 100 years. The most likely orbits for collisions are expected to be in the highly utilised 800 – 1000 km altitude band, at near-polar inclinations (Figure 1.4–2). This accelerating collision activity would generate enough fragments to overwhelm all other debris sources in LEO over the course of the next century. As a consequence, the population of smaller (but still damaging) objects in LEO would exhibit long-term exponential growth (Figure 1.4–3).

Although no collisions were predicted by DELTA in the GEO region, the absence of any natural removal mechanism for debris objects will mean that the population can only increase over time. As such, if the increase in the population continues to remain unchecked over the coming centuries, the onset of collision activity in GEO is to be expected.

It was found that the NaK droplet population, whilst contributing significantly to the current LEO debris environment in the 800 – 1000 km altitude band, would be mostly removed from orbit by atmospheric drag within the next two solar cycles. Slag particles ejected from solid rocket motor firings (particularly apogee boost motors) are predicted to continue to grow and dominate the millimetre debris population in MEO, and both the millimetre and centimetre populations in GEO

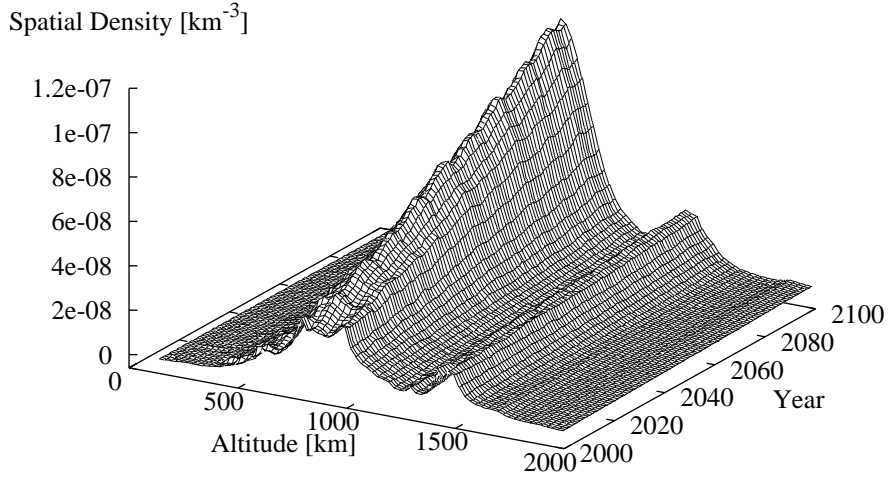


Figure 1.4–1: The spatial density evolution over altitude of all objects in LEO > 10 cm in size for the Business As Usual scenario

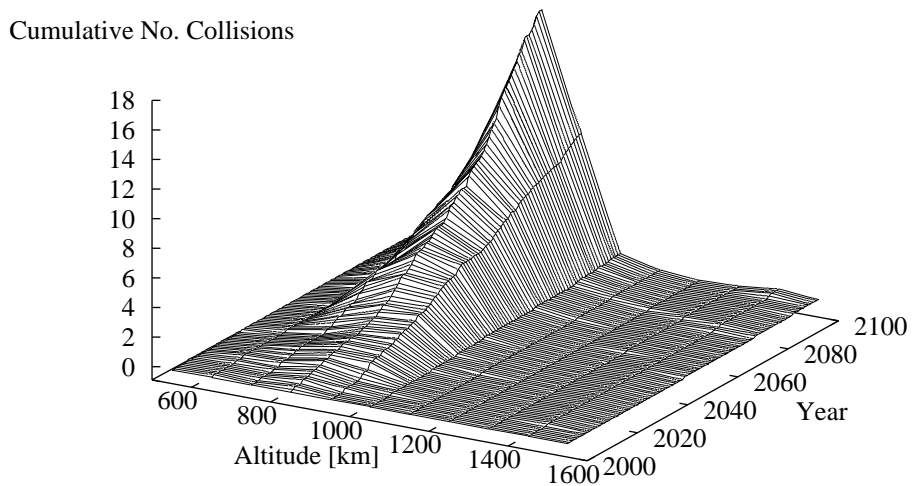


Figure 1.4–2: The cumulative number of collisions in LEO over altitude for the Business As Usual scenario

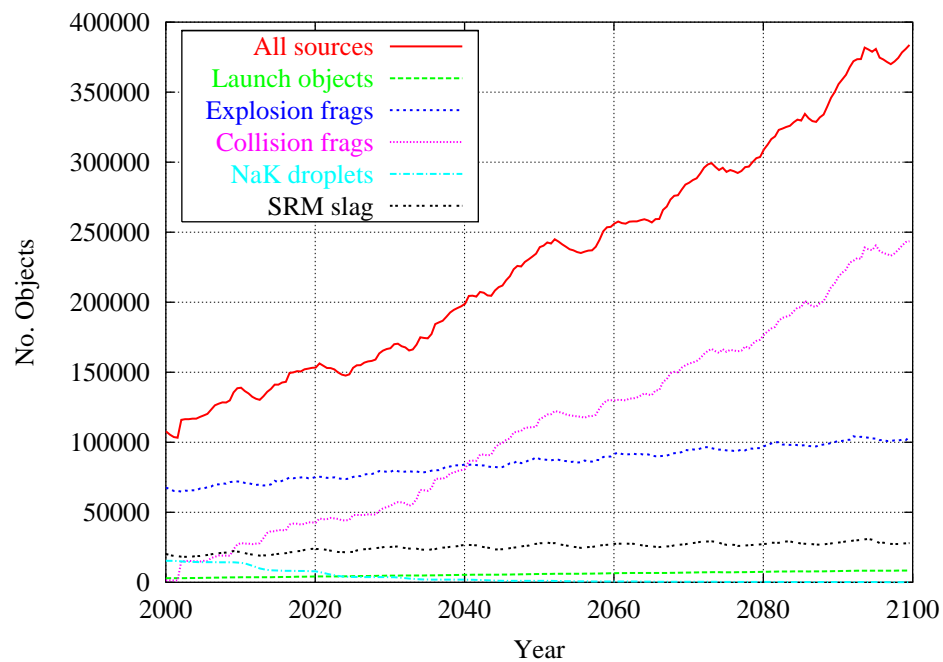


Figure 1.4–3: The evolution of the number of objects in LEO > 1 cm in size broken down by source type for the Business As Usual scenario

in the future according to the simulation. However, there is still no direct observational evidence for these particles at such high altitudes. SRM slag particles are predicted to make a small relative contribution to the future LEO population growth in the Business As Usual scenario.

In order to determine the possible extent of the population growth in the medium and long-term future, it is important to understand the sensitivity of the long-term evolution model to fundamental changes in key model input data and model parameters [10], [11], [12], and [13]. The sensitivity of the ESA DELTA model is assessed in this chapter according to changes in the level of background launch/explosion traffic, the introduction of new satellite constellation systems and nano-satellite swarms consisting of hundreds of spacecraft, and alterations to various aspects of the satellite breakup model.

The long-term evolution of the orbital debris environment is predicted to be highly sensitive to variations in future traffic (launches, explosions and SRM firings). Particularly, if the future traffic rates were to experience a step increase by a factor of two or more, then (without mitigation) the lethal centimetre-sized debris population levels in LEO are predicted to undergo significant exponential growth by an order of magnitude or more over the next century. Such a significant rise in future traffic might be caused by a technology breakthrough such as highly re-useable launch vehicles making frequent low-cost flights to LEO.

The sensitivity study of the long-term LEO debris projections to different constellation traffic was assessed by considering a scenario which simulated the deployment of currently foreseen (launched or planned) constellation systems. The scenario included three successive generations of satellites in each constellation covering an operational period of approximately two decades. These deployments were predicted to have a moderate impact on the long-term evolution of the LEO debris population. However, if a very large constellation is operated in the most crowded orbit for a long period with similar replacement generations, then the debris environment in LEO is predicted to sustain profound, permanent long-term damage.

It was found that the deployment of a nano-satellite swarm consisting of a thousand members into the most crowded region of low Earth orbit would induce a modest, but observable impact on the



future collision rate and hence debris population growth. This is due to the large number of objects orbiting in a narrow altitude band, which significantly increases the localised destructive collision risk to larger objects.

Generally, it has been found that the choice of the different relationships used to simulate an on-orbit fragmentation can be crucial to the outcome of the results produced by a long-term debris environment evolution model. The combination of different number, area-to-mass, and additional velocity distributions over fragment size can have a profound effect on the projected debris population levels over the next century, particularly at smaller debris particle sizes. The most significant influence was observed when the NASA 1998 breakup model [14] was used to generate fragments from explosions and collisions in the DELTA long-term projections. In this case, the NASA breakup model produces many more large and small collision fragments, and many more small explosion fragments compared to the old breakup models used by DELTA throughout the handbook studies, thus leading to significantly higher future population levels for the Business As Usual scenario.

## 1.5 Long-term effectiveness of debris mitigation measures

In order to evaluate the package of mitigation measures providing the most efficient means of preventing significant population growth in the future, the ESA DELTA model has been utilised in this chapter to simulate long-term debris environment evolution in LEO and GEO for various mitigation measure scenarios. Hence, the results and supporting analysis can provide recommendations for space debris mitigation guidelines/standards documents that will be followed by mission/spacecraft engineers. These scenarios include:

- prevention of on-orbit explosions and operational debris release
- reduction of slag debris ejected from solid rocket motor firings
- de-orbiting of space systems in LEO with various limitations on the post-mission lifetime
- re-orbiting of space systems to above the LEO & GEO protection zones

There are three major criteria associated with the evaluation of debris mitigation measures:

### *Benefit*

The package of mitigation measures must be able to stabilise the future collision rate (thereby avoiding collision cascading and future exponential growth of the debris population), and bring population growth under control by achieving stabilised or reduced levels in regions of current high operational value (i.e. LEO and GEO) over the long-term.

### *Risk*

The package of mitigation measures should aim to minimise the collision risk over the long-term by keeping the population levels (i.e. the underlying cause of the collision risk) as low as possible at all altitudes. It is also important to build in a safety margin so the mitigation package can be robust enough to maintain control in the face of unforeseen, significant increases in future spaceflight activity.

### *Cost*

The cost associated with the implementation of the package of mitigation measures should be minimised for future space missions. In relation to post-mission disposal options, the additional propellant required for post-mission disposal manoeuvres of a space system should be minimised.

Clearly, benefit to the space environment is the primary selection criterion, but at what risk and what cost? The risk and cost criteria are clearly two very important, but competing criteria. A relatively lower collision risk in the future will cost relatively more to achieve, and vice versa. Therefore, it is essential to perform a trade-off analysis and strike a balance between them in order to obtain the optimum set of mitigation measures for a recommendation.

It was found from the DELTA long-term projections that the combined implementation of passivation and mission-related object elimination as debris mitigation measures would be unable to prevent an increasing rate of collisions in the LEO region in the future. These measures would also be unable to prevent future debris population growth in both the LEO and GEO regions. The additional post-mission disposal of spacecraft and launch vehicle upper stages is needed in LEO and GEO, thus removing their potential to be involved in any future collision events.

The implementation of solid rocket motor slag prevention measures was found to be an effective measure to mitigate population growth in the GEO region at centimetre and sub-centimetre particle sizes. However, a recommendation for solid rocket slag prevention for the GEO region cannot be currently justified on the basis of a lack of observational data to validate the model results.

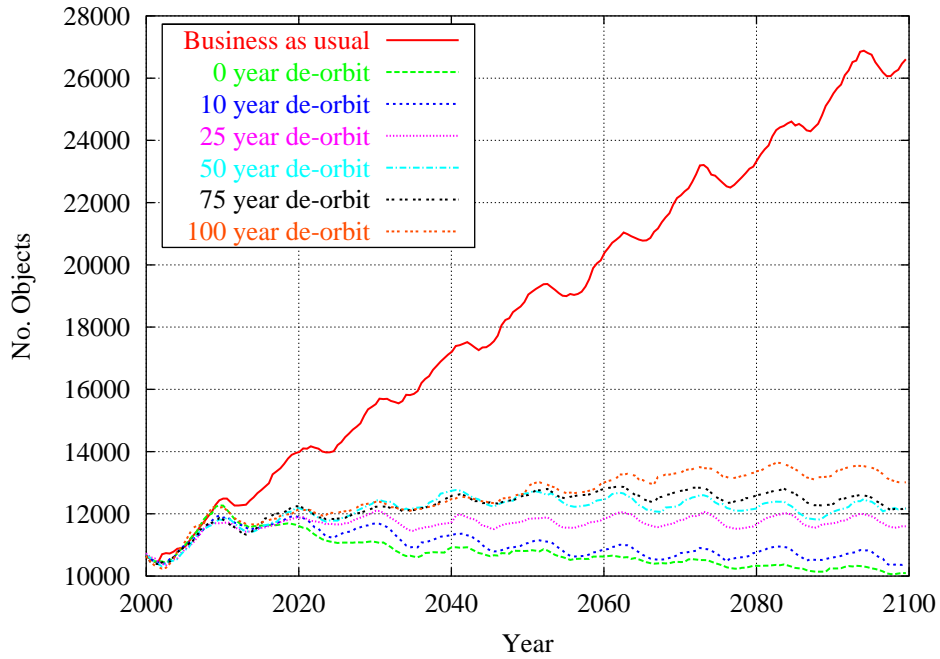


Figure 1.5–1: The evolution of the total number of objects in LEO > 10 cm in size for the different de-orbit scenarios

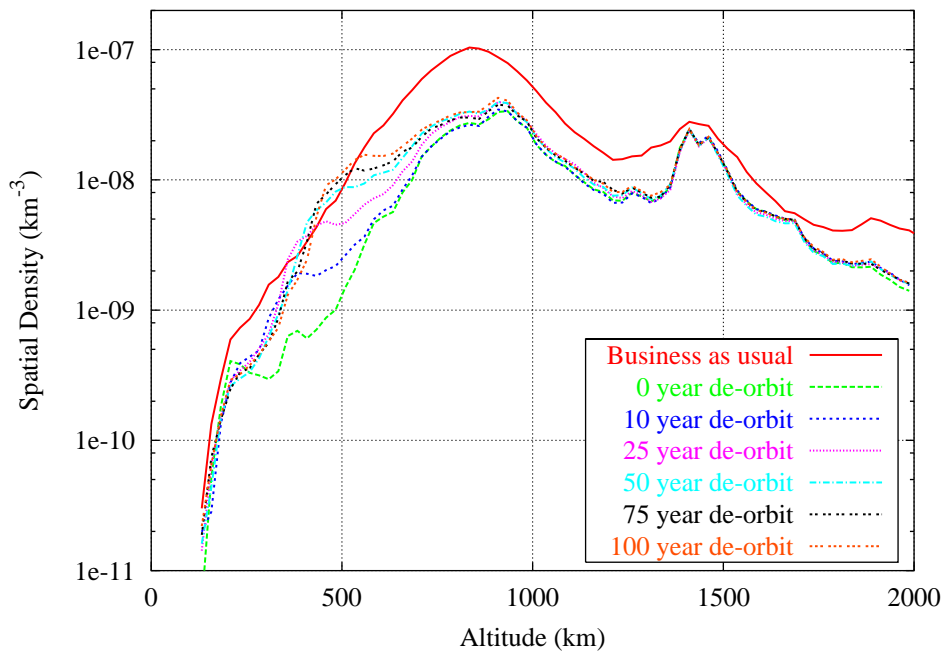


Figure 1.5–2: The spatial density over altitude of all objects in LEO > 10 cm in size after 100 years for the different de-orbit scenarios

Based upon the studies of the long-term effectiveness of different post-mission lifetime limitation policies in reducing future debris growth for nominal and high future launch traffic levels, and upon an analysis of disposal manoeuvre propellant requirements, the following conclusions can be made concerning the post-mission de-orbiting of space systems in LEO:

- Under assumptions of a continuation in recent launch activity into the long-term future, any post-mission de-orbit lifetime limitation policy between 0 and 100 years (in combination with passivation) would be effective in stabilising the future collision rate and future LEO debris population levels.
- The stabilised population level for large objects depends upon the choice of the post-mission lifetime limitation with higher population levels (at altitudes below 800 km) for longer lifetimes and lower population levels for shorter lifetimes (see Figure 1.5–1 and Figure 1.5–2).
- Under assumptions of a sharp increase in the future launch traffic by a factor of two, the post-mission lifetime limitation policies of 25 years or less would be tolerant to such a significant increase in future launch traffic with no loss of effectiveness. Higher post-mission lifetimes, from 50 to 100 years, would be slow to respond to the launch traffic increase and hence unable to maintain the same low population level and low constant collision rate.
- The required disposal manoeuvre propellant increases linearly with a low gradient as post-mission lifetime decreases from 100 years down to 25 years. As the post-mission lifetime decreases further from 25 years down to 0 years, the required manoeuvre propellant grows in an exponential manner. Therefore, a 25-year post-mission lifetime is the shortest possible before propellant requirements start to become disproportionately high.
- The action of space systems lowering their perigee altitude at end-of-life to comply with post-mission disposal lifetime limitations of 25 years or longer can increase the number of trackable objects crossing low altitude manned mission orbits in the long-term. However, the safety of astronauts/cosmonauts would not be compromised due to vigilant object tracking, close approach assessment and collision avoidance procedures. Therefore, this issue is not a significant factor in the selection of a recommended post-mission lifetime rule. Importantly, all of the post-mission lifetime rules considered were able to substantially reduce the collision rate in the main collision region at higher altitudes, thus reducing the collision risk to manned missions from the lethal centimetre-sized debris to below present-day levels.

As a result of the above conclusions, it is recommended that a 25-year post-mission lifetime limit should be implemented, in addition to mission-related object limitation and passivation measures in LEO. This selection represents the optimum balance between benefit to the space environment, minimising collision risk, and minimising the cost of implementation in terms of disposal manoeuvre demands. It is also a robust and durable selection that ensures a sufficient safety margin that maintains its effectiveness in the face of a significant increase in launch traffic in the future.

The de-orbit manoeuvre requirement for a mission operating at 1400 km altitude is high, and therefore the possibility of re-orbiting above LEO was investigated in terms of the potential consequences for the environment (see Figure 1.5–3). At the present time, the DELTA model results suggest that allowing LEO space systems at high LEO altitudes to re-orbit above the LEO protected region of 2000 km will lead to negligible collision activity in the next century. However, due to a lack of atmospheric drag removal at these higher altitudes, re-orbited objects and any fragments from explosions or collision breakups will remain as a long-term collision hazard for many centuries to come, and so the region can easily reach a collision instability through overuse and/or poor passivation. Thus, it is recommended that re-orbiting above LEO should be performed only in exceptional circumstances where de-orbiting is not feasible, and with the proviso that passivation measures are strictly and reliably performed. Re-orbiting above the GEO region is currently the only option, since de-orbiting is not feasible. The DELTA model results have shown that it is an effective measure to stabilise the collision risk in the GEO ring (see Figure 1.5–4). No collisions were predicted by DELTA in the GEO disposal region over the next century.

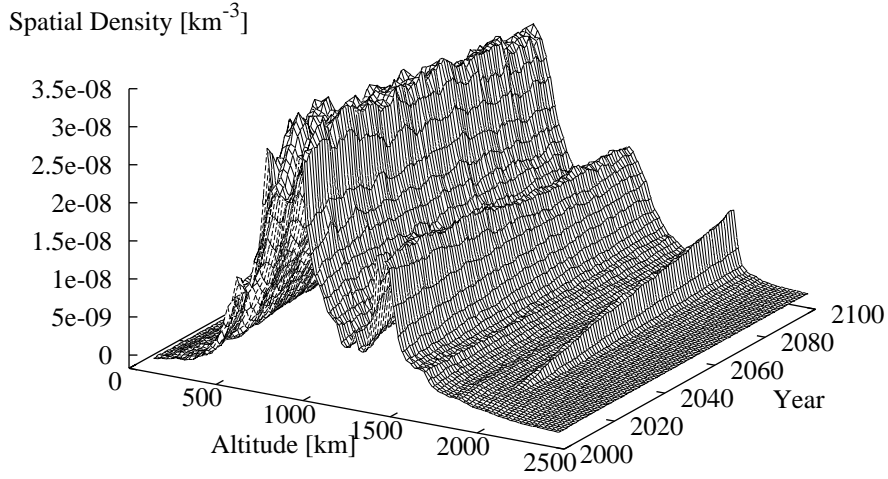


Figure 1.5–3: The spatial density evolution over altitude of all objects in LEO > 10 cm in size for the LEO re-orbiting scenario

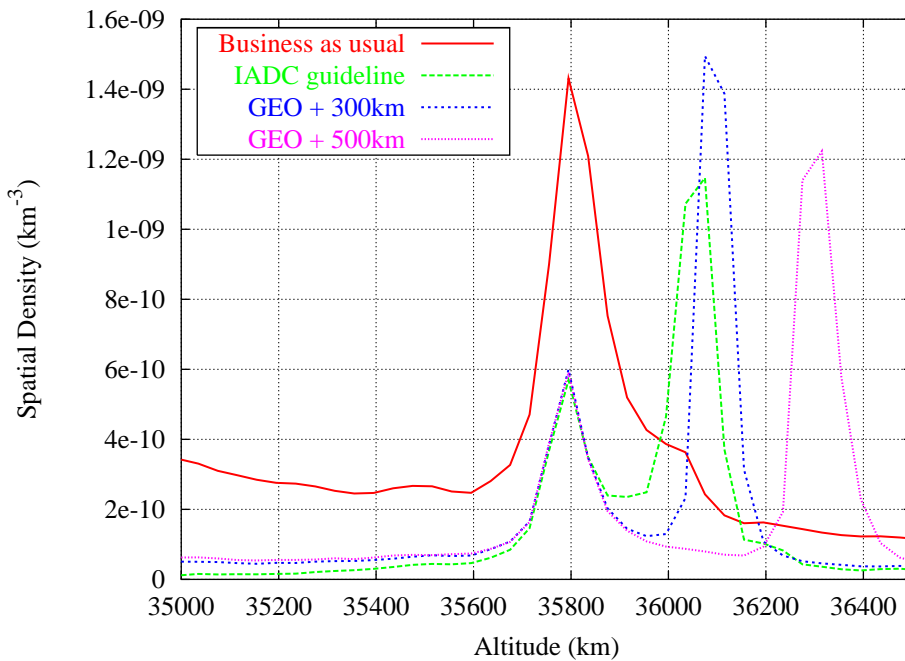


Figure 1.5–4: The spatial density over altitude of all objects in GEO > 10 cm in size after 100 years for the different GEO re-orbiting scenarios

## 1.6 Long-term forecasting of debris impact risk

As awareness of the orbital debris issue continues to spread throughout the space industry, those designing space missions and spacecraft are learning that mission lifetime collision risks are already moderate in some regions of LEO and are on the increase. These risks must be properly assessed in order to make the trade-off against other risk factors to achieve acceptable reliability/system availability figures. If mission lifetime collision risks are unacceptably high, they must be effectively mitigated through changes to the mission (orbit selection) or spacecraft design (shielding). The DELTA model has been designed specifically to perform long-term collision risk evolution predictions and is utilised in this chapter to provide trend forecasts for LEO, GTO and GEO missions operating in the future environments presented in the Handbook.

Two LEO target orbits were selected, corresponding to typical missions – namely a low altitude manned mission at 450 km altitude and 51.5 degrees inclination, and a higher altitude remote sensing mission in a sun-synchronous orbit (98.5 degrees inclination) at 800 km altitude. For the remote sensing mission, the centimetre-sized impact flux is initially dominated by explosion fragments and NaK droplets, but they exhibit low growth and decay respectively and are soon overtaken by the rapidly growing collision fragment source in the region for a Business As Usual scenario. The >10 cm impact flux for the remote sensing mission is initially dominated by explosion fragments and launch-related objects, but large collision fragments may begin to overtake these sources by the end of the century-long period. Therefore, post-mission disposal (when combined with passivation) is the most effective risk mitigation measure for this mission in the long-term, since it stabilises the risk from launch-related objects and stabilises the collision rate.

For the low altitude manned mission, the centimetre-sized impact flux is dominated by SRM slag particles and explosion fragments throughout the 100 year trend prediction period, according to the DELTA results. The collision fragment contribution grows to a similar level after 100 years of evolution. The >10 cm impact flux for this mission is dominated by launch-related objects and explosion fragments decaying through 450 km altitude from above. Therefore, the most effective risk mitigation measures for a low altitude manned mission are passivation, SRM slag prevention and post-mission disposal to reduce the smaller collision fragment population (see Figure 1.6–1). A side effect of post-mission disposal of LEO space systems by lowering perigee altitude to ensure decay within a limited lifetime is that the impact flux from large objects increases along the timescale of the lifetime limitation (e.g. 25 years) and then stabilises at a higher level. The longer the lifetime, the higher the stabilised flux level (see Figure 1.6–2). The stabilised impact flux level for a 25-year de-orbiting rule would only slightly exceed that for a Business As Usual scenario in the next 50 years. Thereafter, it enables a relative risk reduction. Any increase in the population at manned mission altitudes in the next few decades due to de-orbiting does not represent an increase in collision risk, since these large objects can be avoided by the usual object tracking and collision avoidance procedures for manned missions. A 25-year post-mission lifetime policy was found to provide a good compromise between a 100-year lifetime rule with a higher station manoeuvre cost/lower de-orbit cost for higher altitude missions, and a 10-year lifetime rule with a lower station manoeuvre cost/higher de-orbit cost for higher altitude missions.

For a GEO mission (35786 km altitude, inclination 0.1 degrees), the largest contributors to the debris flux are again size threshold dependent. At centimetre sizes, the impact flux to a typical GEO orbit is predicted to be dominated by the slag particles from solid rocket motor firings. Consequently, introducing SRM slag prevention as a mitigation measure is demonstrated to be a very successful method for containing the flux. However, at decimetre sizes the launch-related objects are predicted to be the largest contributor to the impact flux. In this case, removal of space systems from the operational GEO region via re-orbiting to higher altitudes (combined with passivation) is by far the most effective means of controlling the growth in the debris flux. It is important to note that the introduction of passivation measures alone is not predicted to diminish the linear growth of flux over time. Passivation of re-orbited objects is absolutely necessary to avoid the generation of fragments in the disposal region which could be dispersed into the GEO ring.

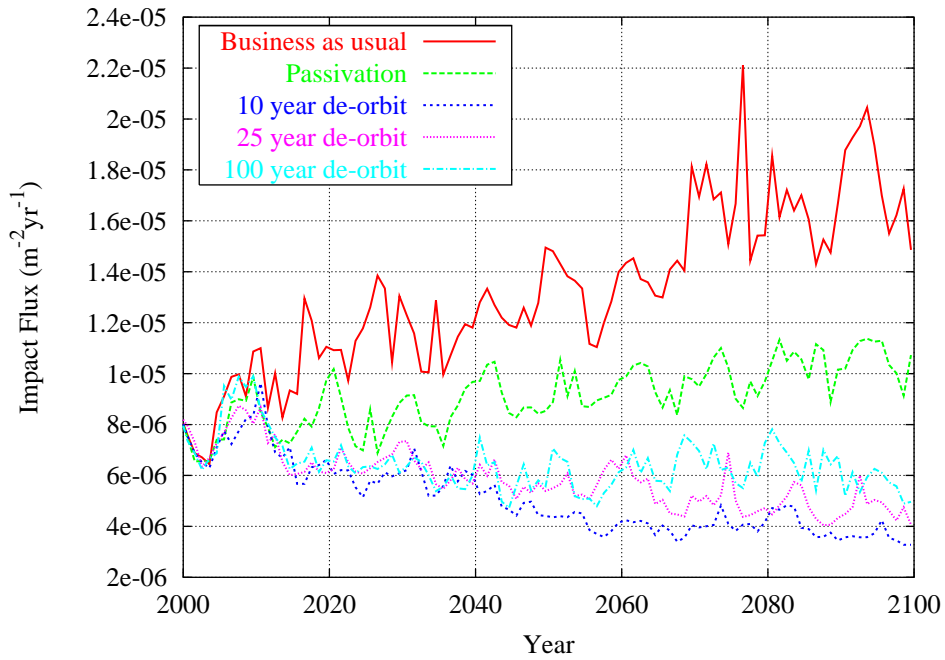


Figure 1.6–1: The total impact flux to the manned mission orbit from all objects > 1 cm in size for the different mitigation scenarios

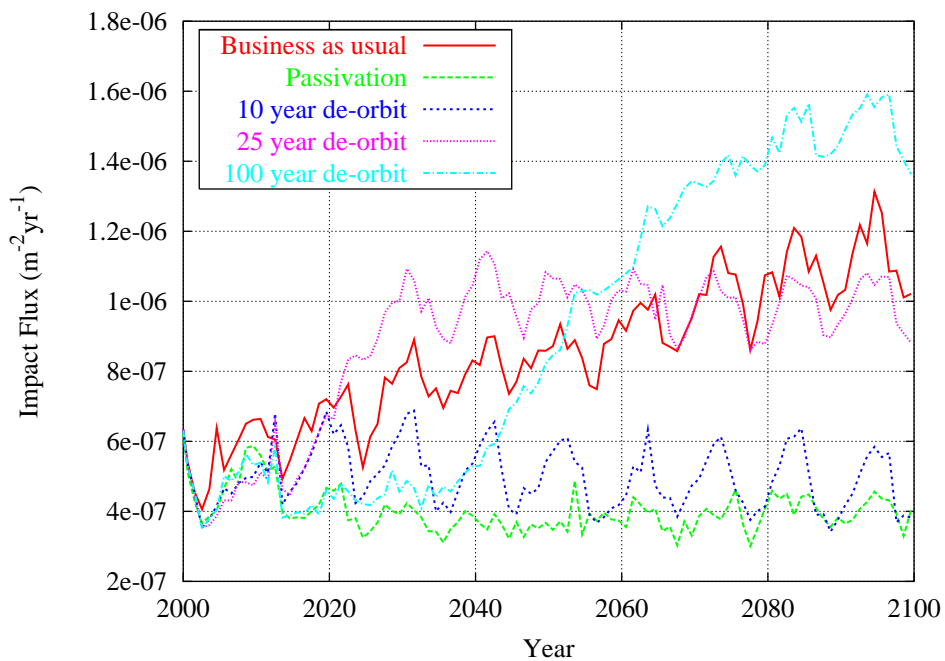


Figure 1.6–2: The total impact flux to the manned mission orbit from all objects > 10 cm in size for the different mitigation scenarios

## 1.7 Debris mitigation guidelines and techniques

National space agencies and International forums, such as the Inter-Agency Debris Co-ordination Committee (IADC), have acknowledged the seriousness and necessity for prompt action regarding the space debris problem, and are continuously researching the subject in an effort to identify beneficial operational and design mitigation practices to protect both space vehicles and the environment. Such recommendations are ultimately intended for future submission to international regulatory bodies such as the UNCOPUOS (United Nations Committee on the Peaceful Uses of Outer Space), and if accepted could eventually be lawfully enforced among the entire space community.

This chapter examines the current guidelines and recommendations to mitigate the debris problem through a comparative review of the main National and International Mitigation Standards documents, namely:

- NASA Safety Standard [15]
- CNES Safety Requirements — Space Debris [16]
- Draft European Space Debris Mitigation & Safety Standard (EDMS) [17]
- NASDA Space Debris Mitigation Standard [18]
- RASA Branch Standard — Space Technology Items [19]
- US Government Orbital Debris Mitigation Standard Practices [20]

Other comparisons of world standards can be found in [21, 22]. The above documents, together with related papers, are compared by considering the following five common categories of debris mitigation measures:

- reduction of mission-related objects (operational debris)
- prevention of accidental explosions (passivation of space systems)
- limiting the effects of intentional breakups
- avoidance of collisions on-orbit and during launcher ascent
- post-mission disposal of space systems (de-orbiting or re-orbiting by chemical/electric propulsion, tethers or drag augmentation)

Practical techniques, methods and procedures to limit debris generation which are currently employed, or proposed for future use are also discussed within the framework of this chapter. For example, suggested passivation procedures include: burn or vent residual propellants and leave fuel lines with valves open; vent all pressurised systems, or include a pressure relief mechanism to ensure no explosion under expected solar heating conditions; discharge batteries, and shut down charging line or include an appropriate design option to ensure a permanent discharge state; deactivate range safety systems; and remove rotation/power from control momentum gyros.

The national debris mitigation guidelines vary widely in their requirements for the post-mission disposal of space systems in the different orbital regimes, such as LEO, GTO, MEO, and GEO. A detailed comparison of national guidelines in this area is provided in Table 1.7–1. Discussions at an international level through the IADC are aiming to reach a common set of recommendations on post-mission disposal and other measures.



	LEO	12hr circular MEO	GTO ( $H_p < 2,000\text{km}$ )	GEO
<b>NASA</b>	<ul style="list-style-type: none"> <li>Direct retrieval within 10yrs.</li> <li>Re-entry within 25yrs.</li> <li>Re-orbit so that: <math>H_p &gt; 2,500\text{km}</math> and <math>H_a &lt; 35,288\text{km}</math>.</li> </ul>	<ul style="list-style-type: none"> <li>Re-orbit so that EITHER: a) <math>H_p &gt; 2,500\text{km}</math> and <math>H_a &lt; 19,900\text{km}</math>, OR b) <math>H_p &gt; 20,500\text{km}</math> and <math>H_a &lt; 35,288\text{km}</math>.</li> <li>Direct re-entry.</li> <li>No requirement for disposal manoeuvre.</li> </ul>	<ul style="list-style-type: none"> <li>Re-orbit so that: <math>H_p &gt; 2,500\text{km}</math> and <math>H_a &lt; 35,288\text{km}</math>.</li> <li>Direct retrieval.</li> <li>Re-entry within 25yrs.</li> <li>Re-orbit so that: <math>H_p &gt; 2,000\text{km}</math> and <math>H_a &lt; R_{\text{GEO}} - \Delta H2</math> km.</li> </ul>	<ul style="list-style-type: none"> <li>Re-orbit above GEO by a distance, <math>\Delta H1</math>: <b>300km + <math>(1000 \times A/m)\text{km}</math></b></li> <li>Re-orbit above GEO by a distance, <math>\Delta H2</math>: <b>235km + <math>(1000 \times C_R \times A/m)\text{km}</math></b></li> </ul>
<b>CNES &amp; Draft EDMS</b>	<ul style="list-style-type: none"> <li>Direct re-entry.</li> <li>Re-entry within 25yrs.</li> <li>Re-orbit so that: <math>H_p &gt; 2,000\text{km}</math> and <math>H_a &lt; R_{\text{GEO}} - \Delta H2</math> km.</li> </ul>	<ul style="list-style-type: none"> <li>Re-entry within 25yrs.</li> <li>Re-orbit so that EITHER: a) <math>H_p &gt; 1,700\text{km}</math> and <math>H_a &lt; 19,900\text{km}</math>, OR b) <math>H_p &gt; 20,500\text{km}</math> and <math>H_a &lt; 35,288\text{km}</math>.</li> </ul>	<ul style="list-style-type: none"> <li><math>H_a</math> of upper stages should be reduced to <math>&lt; H_{\text{GEO}} - 500\text{km}</math> within 25yrs.</li> </ul>	<ul style="list-style-type: none"> <li>Re-orbit above GEO by a distance, <math>\Delta H3</math>: <b>200km + <math>(0.022 \times a \times C_R \times A/m)\text{km}</math></b></li> </ul>
<b>NASDA</b>	<ul style="list-style-type: none"> <li>Direct retrieval.</li> <li>Re-entry within 25yrs.</li> <li>Re-orbit so that: <math>H_p &gt; 1,700\text{km}</math> (preferably 2,500km).</li> </ul>			
<b>RASA</b>	General requirement to reduce orbital lifetime of spacecraft or booster module after EOL.			
<b>US Gov.</b>	<ul style="list-style-type: none"> <li>Direct retrieval as soon as practical after EOL.</li> <li>Re-entry within 25yrs.</li> <li>Re-orbit so that: <math>H_p &gt; 2,000\text{km}</math> and <math>H_a &lt; 19,700\text{km}</math>.</li> </ul>	<ul style="list-style-type: none"> <li>Re-orbit to one of the following disposal zones: a) <math>H_p &gt; 2,000\text{km}</math> and <math>H_a &lt; 19,700\text{km}</math>, b) <math>H_p &gt; 20,700\text{km}</math> and <math>H_a &lt; 35,300\text{km}</math>.</li> </ul>	<ul style="list-style-type: none"> <li>Re-orbit to one of the following disposal zones: a) <math>H_p &gt; 2,000\text{km}</math> and <math>H_a &lt; 19,700\text{km}</math>, b) <math>H_p &gt; 20,700\text{km}</math> and <math>H_a &lt; 35,300\text{km}</math>, c) <math>H_p &gt; 36,100\text{km}</math>.</li> </ul>	<ul style="list-style-type: none"> <li>Re-orbit above GEO by a distance: &gt; <b>200km</b> (taking account of the evolution of the space vehicle from various orbital perturbations).</li> <li>Re-orbit <math>\sim 300\text{km}</math> above GEO so that <math>H_p &gt; 36,100\text{km}</math>.</li> </ul>

Table 1.7-1: Summary of Proposed Post-mission Disposal Options ( $H_p$  = Perigee altitude (km);  $H_a$  = Apogee altitude (km))

## 1.8 Post-mission disposal assessment

### Orbital lifetime analysis

The orbital lifetimes of objects passing through the densely populated LEO environment can be many thousands of years for near circular orbits of a high mean altitude, or for highly eccentric orbits. A limitation of the post-mission orbital lifetimes of spacecraft and upper stages passing through LEO with large masses and cross-sections is necessary in order to avoid an accumulation of large objects, and in order to inhibit a further growth of smaller debris due to explosions and collisions. An upper limit for remaining orbit lifetimes of 25 years after mission completion is currently being discussed at an international level as a design guideline for operators releasing spacecraft and upper stages into orbits which cross the LEO environment. Such lifetime limitations could be implemented in future spacecraft designs by means of active post-mission de-orbiting into a direct or delayed re-entry, or by the exploitation of natural perturbations in concert with properly selected post-mission orbital conditions.

The orbital lifetimes of spacecraft and upper stages, both of which are characterised by relatively large mass-to-area ratios, are determined by the following parameters and orbital perturbations:

- atmospheric drag: depending on the mass-to-area ( $m/A$ ) ratio of the object, on the perigee altitude, shape, and orientation of the orbit, and on atmospheric state parameters (the most important being the solar activity, which varies in an 11-year cycle)
- solar radiation pressure: depending on the mass-to-area ratio ( $m/A$ ) of the object, and on the perigee altitude, shape, and orientation of the orbit with respect to the Sun and to the Earth shadow
- luni-solar perturbations: depending on the perigee altitude, shape, and the orientation of the orbit with respect to the Sun and the Moon (relevant mainly for highly eccentric orbits)

Fig. 1.8–1 shows expected orbital lifetimes of near-circular LEO orbits. For the lifetime prediction a constant medium solar activity was assumed ( $F_{10.7} = 125 \cdot 10^{-22} \text{ W/m}^2/\text{Hz}$ ), averaged over one representative solar cycle). This means that the lifetime values are valid for this solar activity only, if they are less than one solar cycle. Thus, for orbits of shorter lifetimes, the predicted solar activity variation has to be considered.

Lifetime results are not given directly, but related to the mass-to-area ratio as a function of the initial perigee altitude. Each curve is valid for the specified (initial) eccentricity. In order to determine the lifetime of an object, the quantity read from the ordinate has to be multiplied by the mass-to-area ratio.

Example: The orbital lifetime of a satellite with the following parameters:

- mass-to-area ratio:  $100 \text{ kg/m}^2$ ,
- (initial) perigee altitude:  $450 \text{ km}$ ,
- (initial) eccentricity:  $0.01$

is approximately 3 years.

For ESA's ERS-1 and ERS-2 spacecraft, with near circular orbits of about 780 km mean altitude, and mass-to-area ratios of about  $75 \text{ kg/m}^2$ , lifetimes of more than 100 years can be expected, unless the spacecraft are placed into reduced lifetime orbits by lowering their perigee at the end-of-mission. Preliminary analysis for the French SPOT-1 satellite (which operates on an ERS-like orbit) showed that a reduction of the perigee altitude to about 300 km by means of successive apogee burns would

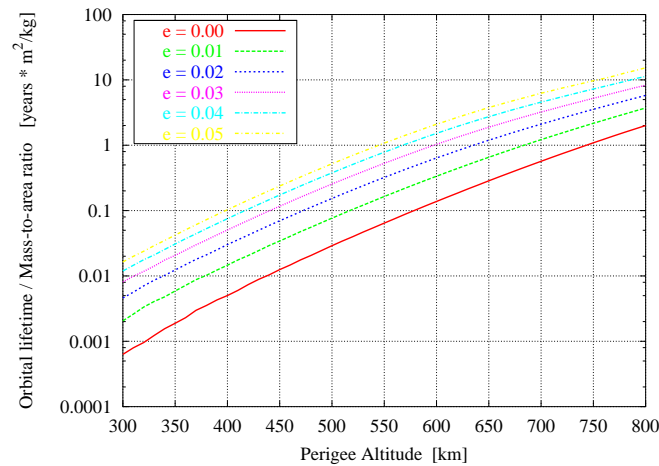


Figure 1.8-1: *Orbital lifetime of LEO objects*

reduce the remaining orbital lifetime to less than 5 years. A further active reduction of the perigee altitude will most probably be inhibited by a loss of the attitude due to perturbing aerodynamic moments. The final decay will thus be uncontrolled.

The current man-made objects population contains about 360 000 objects with diameters larger than or equal to 1 cm. Figure 1.8-2 depicts the distribution of the orbital lifetimes of these objects.

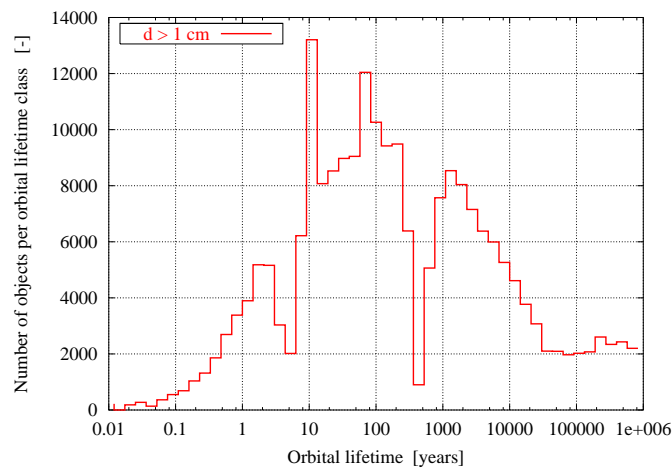


Figure 1.8-2: *Distribution of the orbital lifetimes of the population > 1 cm*

Generally, it can be stated, that only a small number of objects has lifetimes below a few months and above approximately 30 000 years. This distribution is also observed for the catalogued objects population as stored in the DISCOS database (refer to [6]). The majority of the considered objects (> 1 cm) has lifetimes of 10 years up to 10 000 years.

### Propulsive manoeuvre estimates for an uncontrolled de-orbit

If the risk of on-ground human casualty of a space mission has been determined to be lower than a given threshold value, then an uncontrolled, later re-entry of the space vehicle is deemed to be acceptable. In this case, the impact location of any surviving fragments during the re-entry is not important, and therefore the operator may choose to lower the orbit so that atmospheric drag

ensures that the vehicle re-enters within a given post-mission lifetime limit, such as 25 years. The orbit-lowering will usually be conducted at end-of-life by using an on-board propulsion system - either chemical or electric thrusters - to perform the manoeuvres required.

The extent of the orbit-lowering manoeuvre, the required change in orbital velocity and the fuel consumed by typical chemical and electric propulsion systems is investigated in this chapter for different post-mission lifetime limits, mission altitudes and space system physical characteristics (mass-to-area ratio). This parametric analysis has been performed in order to:

- determine the manoeuvre requirements for different post-mission lifetime limitation policies (relating to typical LEO mission altitudes), and therefore support the selection of a recommended, cost-effective post-mission lifetime limit;
- determine the manoeuvre requirements for different LEO mission altitudes (relating to a post-mission lifetime of 25 years), and therefore provide reference data to mission designers for use in the planning of de-orbit manoeuvres and mission trade-off studies.

To allow a comparison of the capabilities of chemical and electric propulsion systems to de-orbit spacecraft on near-circular orbits in the LEO region, a basic software tool DEORBITER has been developed. The calculation of disposal orbit perigee altitude for each spacecraft or upper stage reaching end-of-life assumed a constant average solar activity value of 120 solar flux units when obtaining atmospheric density and density scale height at a given altitude.

The DEORBITER results show that electric propulsion systems consume nearly an order of magnitude less fuel (in terms of mass) than chemical propulsion systems to de-orbit the spacecraft to the required post-mission lifetime orbit (see Figures 1.8–3 and 1.8–4). This is particularly significant for high altitude LEO missions (e.g. 1400 km altitude) where the chemical fuel mass fraction is on the order of 8 to 11%. In addition, electric propulsion system hardware is often lighter than chemical systems. However, the net effect of fuel mass savings plus extra costs to achieve a reliable de-orbit manoeuvre will be one of the main determining factors for the selection of electric propulsion over chemical propulsion for the de-orbit of different spacecraft configurations and mission profiles in LEO.

The influence of the exponential atmospheric density profile can be seen in all of the DEORBITER results for both chemical and electric propulsion de-orbiting. Given an exponentially decreasing atmospheric density (and therefore drag force) with increasing altitude, the orbital decay lifetime exponentially increases. Conversely, exponentially lower perigee altitudes will be required to meet decreasing post-mission lifetimes. The consequence of this is an exponentially increasing delta-velocity and fuel requirement for decreasing post-mission lifetimes. One important aspect of the fuel mass margin distributions over post-mission lifetime is that this exponential characteristic is only noticeable for post-mission lifetimes of less than 25 years (see Figures 1.8–3 and 1.8–4). The reduction in post-mission lifetime from 100 years down to 25 years requires only a low gradient linear (or near-linear) increase in fuel mass fraction.

Hence, 25 years has been found to be the shortest possible post-mission lifetime that can be achieved without disproportionate increases in the fuel requirement for de-orbiting.

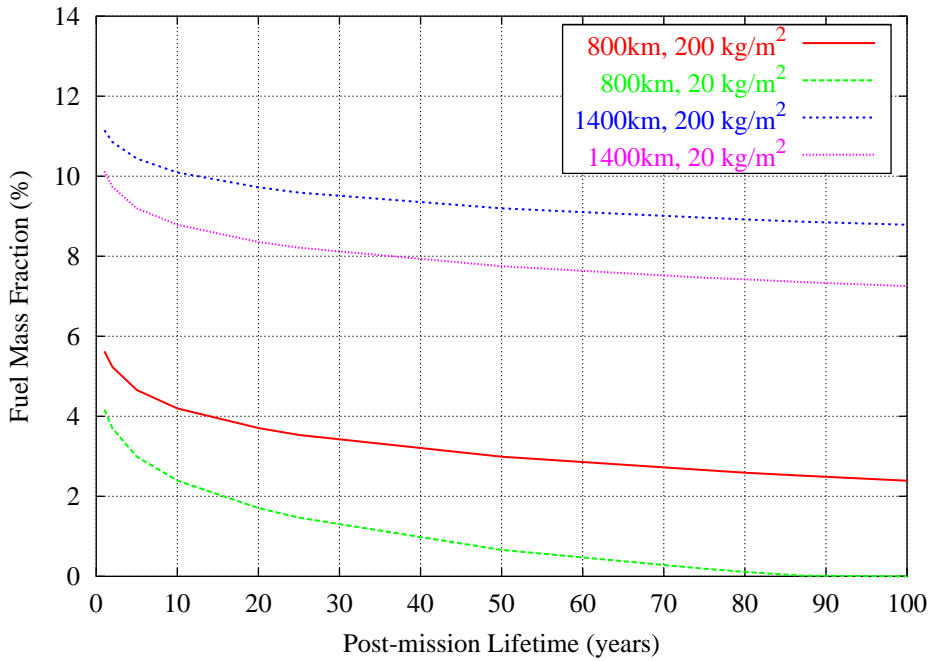


Figure 1.8–3: Fuel mass fraction versus post-mission lifetime for chemical propulsion

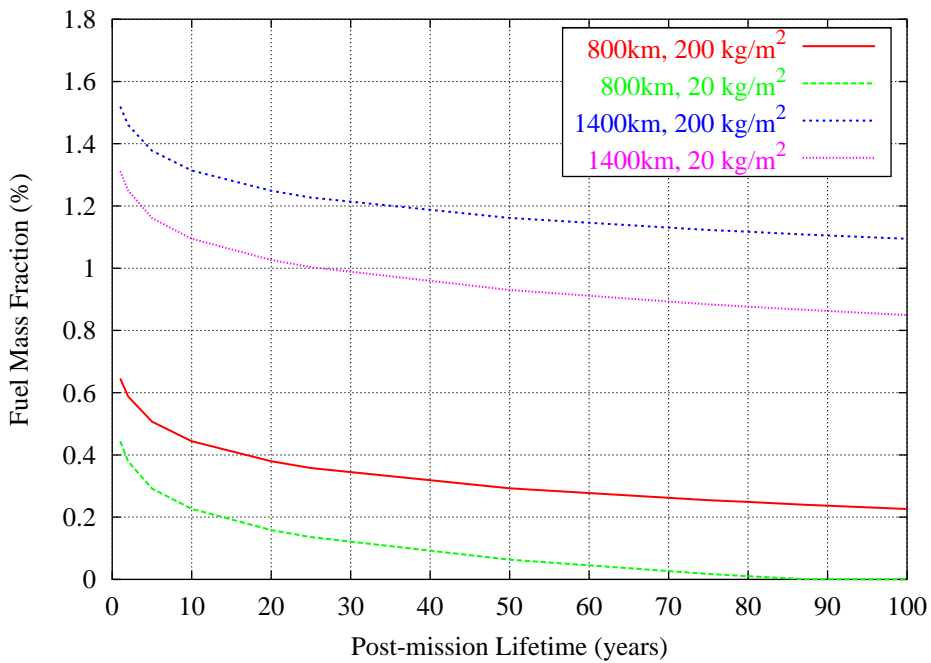


Figure 1.8–4: Fuel mass fraction versus post-mission lifetime for electric propulsion

## 1.9 Re-entry survivability and on-ground risk assessment

One of the key issues in re-entry risk analysis is the identification of components of a spacecraft which are likely to survive the deceleration and heating peaks following a break-up event at altitudes of typically 75 to 80 km. Studies by NASA [23] and ESA [24] & [25] have addressed this task, which involves a simultaneous solution of 3 or 6 degrees-of-freedom (DoF) flight dynamics equations, with aerodynamic, aerothermodynamic, thermal, and structural loads acting on a complicated geometry, composed of many different materials, with properties which need to be defined over a wide temperature range. For simple shapes of given material properties, and for 3 DoF flight dynamics (no attitude propagation), results of different numerical prediction tools can be validated analytically.

In [26] simple, solid shapes (i.e. spheres, cylinders, and disks) made of typical spaceflight materials (i.e. Titanium, stainless steel, Inconel, Aluminium, and Copper) are analysed for the re-entry survivability by means of analytical methods, assuming a perfectly heat conducting material. A complete demise of an object is assumed, if the equilibrium temperature  $T_{eq}$  at the time of peak heat flux exceeds the melting temperature  $T_m$ . One can show [26] that in free-molecular flow the demise condition is not depending on body size, whereas in laminar continuum conditions it is. All other dependencies on ambient conditions, trajectory, and material remain unaffected. Fig.1.9–1 shows the result of a numerical computation of demise altitudes of solid spheres as a function of object diameter and material (Ti, Fe, Al, Cu, and inconel). For a given material the demise altitude varies with the object shape. Below a certain minimum diameter  $d < d_{min}$  and above a certain maximum diameter  $d > d_{max}$  the objects tend to survive the re-entry. For  $d < d_{min}$  this is due to the low area-to-mass ratio (since  $A/m \propto 1/d$ ), and due to the resulting early deceleration at high altitudes, with free-molecular heating, and with good re-radiation capabilities (since the ratio re-radiation to heat storage goes with  $A/m \propto 1/d$ ). In case of large objects where  $d > d_{max}$ , the altitude of peak heat flux is lowered into the laminar flow regime. In this case, the increased heat storage capacity (which goes with  $m/A \propto d$ ) and the reduced integrated heat flux allows the object to survive. Titanium has the best survival potential, followed by stainless steel, inconel, and Copper. Due to its low melting temperature and poor re-radiation capability Aluminium has the lowest probability of survival. Above a lower threshold, and below an upper size threshold of a few cm (which is less material dependent), all solid objects tend to burn up. This is an important finding, since most screws, nuts, and bolts used in spacecraft and rocket manufacturing fall into this domain. For the terminal velocity of solid spheres at ground impact the proportionality  $V_{imp} \propto \sqrt{m/A} \propto \sqrt{d}$  holds. Hence, the small survivor objects tend to carry a low risk potential due to their very low impact velocities ("rain down" of small particles). Objects which fall outside the right end of the demise range indicated in Fig.1.9–1 must be analysed in more detail, e.g. by ESA's SCARAB tool.

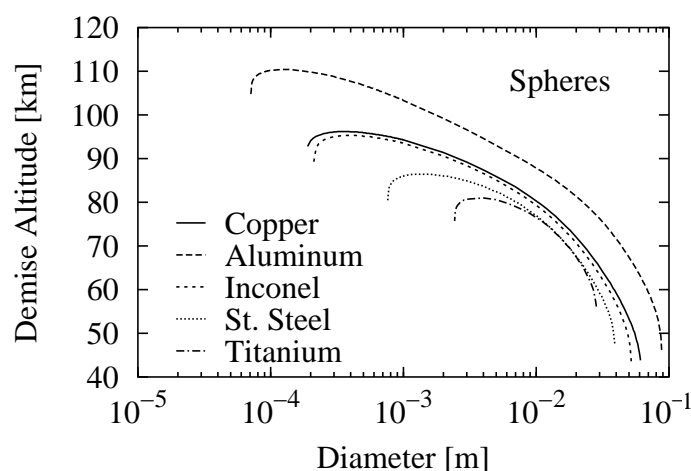


Figure 1.9–1: Demise altitudes of solid spheres as a function of diameter and material.

Of more than 27,000 Earth orbiting objects which USSPACECOM has tracked since 1957 more than 18,000 have re-entered into the atmosphere by the year 2001. Most of these objects disintegrated and burnt up, posing only a minor risk on ground. Occasionally, however, at rates of one in several years orbital structures re-enter, which have geometric cross-sections of 100 m<sup>2</sup> or more, and masses of several 10 tons. Such spacecraft can be classified as high-risk objects. The latest, most massive object in space history to re-enter was Mir (on 23-Mar-2001, with a mass of 135 t). The risk associated with the re-entry of a hazardous object can be assessed, based on empirically justified and computationally verified assumptions on the break-up altitude, and on the cross-track and along-track extension of an impact probability distribution. Population density maps with sufficient spatial resolution are necessary to associate the impact of re-entry survivor objects with a casualty risk in the affected groundtrack swath.

By the year 2000, the world population had reached  $6.23 \times 10^9$ . This value is predicted to double within the next 40 years. Only 11.7% of the world population, and only 33.3% of the land masses are located south of the equator. A re-entry which occurs on the northern hemisphere carries a 1.75 times larger risk than a global mean event. The corresponding risk reduction for a re-entry in the southern hemisphere is by a factor of 1/4.30. This result is directly related to the corresponding mean population densities which are 12.3/km<sup>2</sup> for the whole world, 21.6/km<sup>2</sup> for the northern hemisphere, and 2.9/km<sup>2</sup> for the southern hemisphere (in the year 2000).

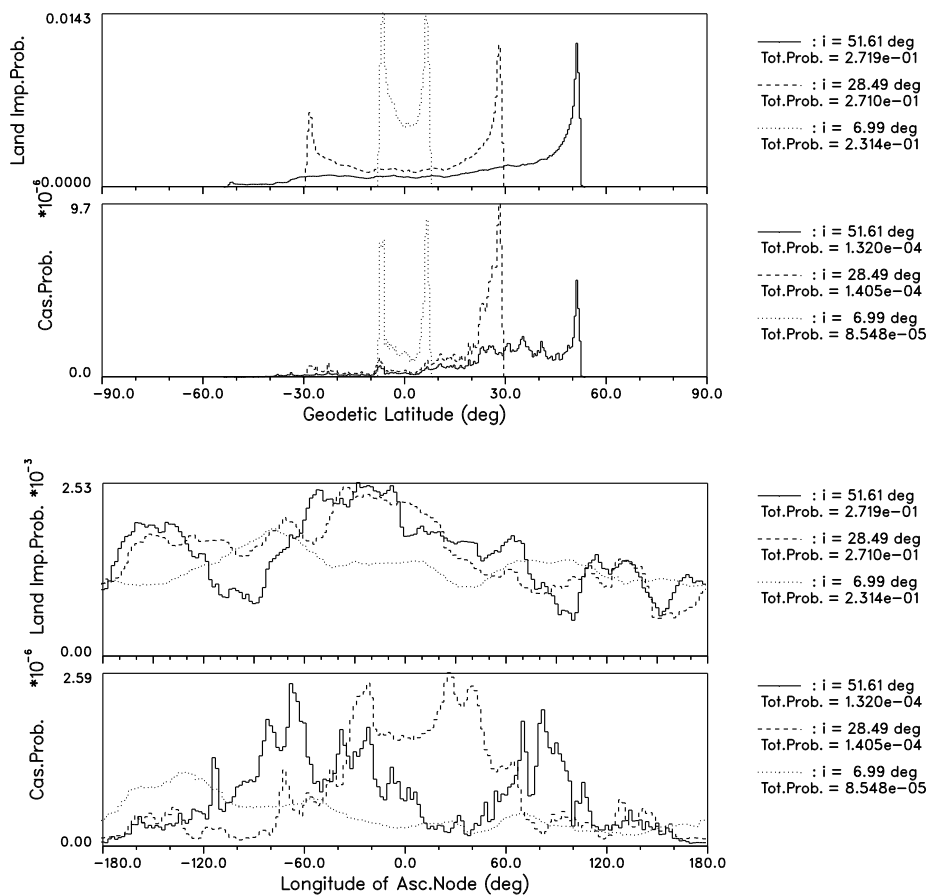


Figure 1.9-2: Land impact probability and casualty probability as a function of geodetic latitude (0.5° bins, top charts), and geographic longitude (2° bins, bottom charts), for orbit inclinations of 7.0°, 28.5°, and 51.6°. For casualty probabilities the 1994 population, and a reference casualty cross-section of  $A_c = 10\text{m}^2$  were assumed.

In order to assess the on-ground risk due to surviving debris of a single re-entry event, the NASA safety standard [27] NSS 1740.14 introduces an equivalent casualty cross-section  $A_c$ , which is composed of the cross-sections  $A_i$  of individual fragments, with each of them augmented by a projected human risk cross-section of  $A_h = 0.36\text{m}^2$  (corresponding to  $\sqrt{A_h} = 0.6\text{m}$ ). When assuming a vertical fall with an immediate rest upon impact, then the resulting effective cross-section for the  $i$ -th fragment is a circle of radius  $r_{c_i} = r_i + r_h$  which circumscribes two touching circles of areas  $A_i = \pi r_i^2$  and  $A_h = \pi r_h^2$ . The total casualty cross-section is then determined by a summation over all  $n$  survivor fragments of a re-entry event. This casualty cross-section can be adjusted for slide, bounce, and non-vertical impact of fragments. The quantity  $A_c$  is a simple, yet very efficient way to concentrate the entire knowledge on the break-up process of a re-entering spacecraft into a single figure.

The highest impact probability  $P_i$  occurs close to the extreme latitudes which can be reached by a given orbit inclination  $i$ , where  $\phi \approx \pm i$ . After weighting of  $P_i$  with underlying land masses, the resulting land impact probability  $P_l$  shows a strong North-South latitude asymmetry. This imbalance towards the northern hemisphere is further emphasised after weighting of  $P_l$  with local population densities to obtain a casualty probability  $P_c$  (for an assumed spacecraft casualty cross-section of  $A_c = 10\text{m}^2$ ). The highest risk concentration of all analysed inclinations can be observed for  $i = 28.5^\circ$  at the northern latitude limit of the related groundtrack pattern for eastward launches from Kennedy Space Center (see Fig.1.9–2, top charts). Tab.1.9–1 summarises the global mean land impact probabilities  $\bar{P}_l$  and casualty probabilities  $\bar{P}_c$  (for  $A_c = 10\text{m}^2$ ) as a function of the orbital inclination, for the selected sample orbits. The procedures for the derivation of impact probability, land impact probability, and casualty probability are explained in detail in the Handbook.

$i$	$7.0^\circ$	$28.5^\circ$	$51.5^\circ$	$65.0^\circ$	$80.0^\circ$	$90.0^\circ$	$98.5^\circ$
$\bar{P}_l$	0.231	0.271	0.272	0.288	0.330	0.333	0.332
$\bar{P}_c$	$8.55 \times 10^{-5}$	$14.1 \times 10^{-5}$	$13.2 \times 10^{-5}$	$9.86 \times 10^{-5}$	$8.54 \times 10^{-5}$	$8.32 \times 10^{-5}$	$8.42 \times 10^{-5}$

Table 1.9–1: Global mean land impact probability  $\bar{P}_l$  and casualty probability  $\bar{P}_c$  (assuming a  $10\text{m}^2$  casualty cross-section  $A_c$ ), as a function of orbital inclination  $i$ .

Due to the stable inclination of Earth orbits, a latitude-oriented risk analysis can be performed very early in the satellite lifetime. A more detailed longitude-oriented risk analysis, closer to the end of the orbital lifetime, allows a further, significant reduction of the re-entry casualty risk. Fig.1.9–2 shows land impact probability and casualty risk results, averaged over single orbit revolutions, as a function of the geographic longitude of the ascending node  $\lambda_n$ , for the orbit inclinations  $7.0^\circ$ ,  $28.5^\circ$ , and  $51.5^\circ$ . A clear concentration of the casualty risk at certain values of  $\lambda_n$  is noticeable, with the positions and amplitudes of the maxima changing with inclination. This knowledge can be used to target re-entry orbits towards longitudes of minimum risk, if the spacecraft has a residual manoeuvring capability (as was the case for Skylab).

A casualty probability of  $P_c < 1:10,000$  per entry event is a figure which is proposed by NASA [28], and which is also proposed (but not yet endorsed) for ESA projects. This number appears to be an analytically justified balance between current risk levels (for today's world population) on the one hand, and technically feasible mitigation and control measures on the other hand. The casualty risk  $P_c$  for a given entry event can be reduced below a given limit  $(P_c)_{max}$  by controlling the casualty cross-section  $A_c$  for the re-entering object (by engineering in the early design phase), by selecting the re-entry area (and hence the underlying population density), or by a combination of both strategies. If one assumes an accepted casualty probability of  $P_c \leq 1:10,000$  per re-entry event, then Fig.1.9–3 shows how much casualty cross-section  $A_c$  may reach the ground for a given orbital inclination. The ratios  $A_c^{(max)}(i)/A_c^{(min)}(i)$  may be on the order of 1,000 for some inclinations. For typical space station orbits near  $i = 50^\circ$  (e.g. Skylab, Salyut-7 and ISS) this ratio between maximum and minimum disposable casualty cross-section is still on the order of 50. Hence, a control of the nodal longitude of the final orbit can greatly reduce the on-ground risk, or (for a given tolerated



risk level) increase the allowed casualty cross-section. When looking at the mean allowed  $A_c$  for  $P_c < 1:10,000$  (see Fig.1.9–3), averaged over all inclinations, and all nodal longitudes, then  $\bar{A}_c$  is close to  $8 \text{ m}^2$  for the year 2000. This is the limit stipulated by NASA in [27] for an uncontrolled re-entry. Hence,  $A_c < 8 \text{ m}^2$  and  $P_c < 1:10,000$  are equivalent requirements for this epoch. In order to be unambiguous, however, it is recommended to adopt the limit on  $P_c$ .

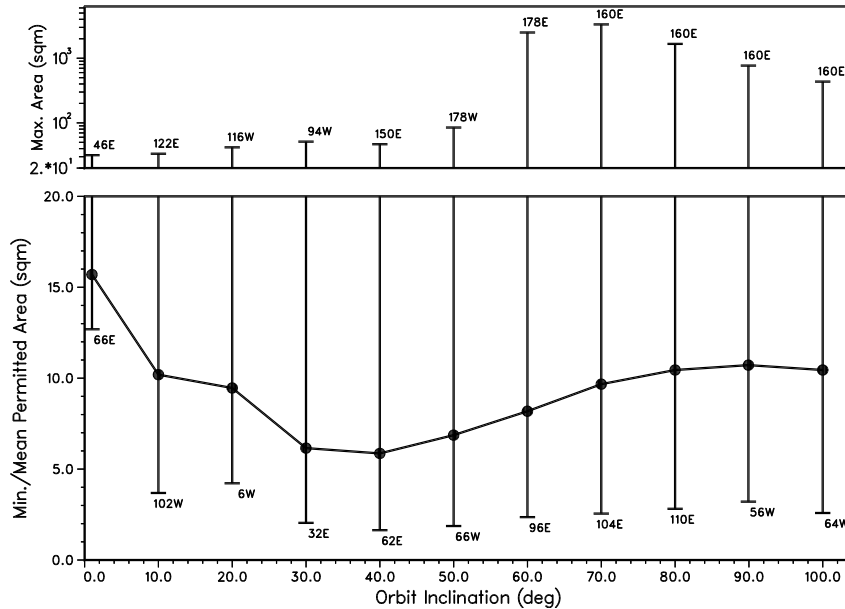


Figure 1.9–3: Ranges of permitted casualty cross-section (minimum, mean, and maximum) for an accepted risk of 1 in 10,000 per event, and for near-circular re-entry orbits, as a function of inclination. The mean accepted cross-section (connected dots) is averaged over 180 orbits, equidistantly spaced in longitude of ascending node (at  $\Delta\lambda = 2^\circ$ ). The minimum and maximum accepted cross-sections are single-orbit averages for the indicated nodal longitude. The world population of 2000 was assumed.

Apart from the primary risk to be hit by spacecraft fragments which have survived the aerodynamic heating during re-entry, some spacecraft can pose a secondary risk due to a possible dispersion of radioactive and/or poisonous material on ground and/or in the lower atmosphere. Two different types of nuclear power sources (NPS) have been used in space missions since 1959: radioisotope thermo-electric generators (RTGs), and nuclear reactors. Between 1965 and 1987, 36 space reactors using  $^{235}\text{U}$  for their fission process had been deployed. Close to 1,500 kg of  $^{235}\text{U}$  nuclear inventory is still in LEO orbits, mostly at 900 km to 1,000 km altitudes. The risk posed by nuclear reactors in space is mainly due to fission products of different half-lives which have been created during the operation of the reactor. Radio-isotope power sources (thermo-electric or thermal generators), also denoted as RTGs, have been used in Earth orbits between 1961 and 1976, and in Earth escape missions since 1969 [29]. The total mass of the RTG nuclear fuel in Earth orbit today is on the order of 150 kg, at altitudes predominantly around 1,000 km. Radio-isotope generators have a radioactive inventory even if they have not been operated.

In the aftermath of the Kosmos-954 re-entry, the United Nations have adopted a set of principles as to the use of nuclear power sources in space [30]. Some of these principles also address the risk potential and liability issues in case of a re-entry.

## 1.10 On-Orbit collision avoidance assessment

At present (in the year 2002), the mean time between collisions of members of the trackable Catalog population is on the order of 10 years, if no avoidance manoeuvres are executed. While the share of controlled spacecraft is only about 6% of the Catalog, their sometimes sizeable masses would yield large fragment clouds during a catastrophic collision, which will have an adverse impact on the orbital environment. Hence, evasive manoeuvres are recommended, if conjunction events, and related collision risks can be predicted with sufficient accuracy. In order to associate a predicted miss distance between any two catalog objects with a corresponding collision risk, the uncertainty of the predicted positions of the objects has to be considered. This position uncertainty can be expressed in terms of a combined  $1\sigma$  error ellipsoid of the chaser and target object at the time of closest approach. The size of the error ellipsoid depends on the orbit determination and prediction uncertainties, and prediction timespan.

For a given extension of the combined target and chaser position uncertainty ellipsoid at conjunction epoch, the collision risk is a function of the fly-by geometry, and of the combined collision cross-section of both objects, which can be assumed to be a circle of diameter  $d_{coll}$  and area  $A_{coll}$ , which encloses the areas of both objects, as projected onto a plane which is perpendicular to the relative velocity vector (so called "B-Plane"). Depending on the length of the propagation arc from orbit determination epoch to conjunction epoch (even for the same fly-by distance and geometry), collision probabilities will be different: The closer in time a conjunction is, the smaller its position uncertainty ellipsoid will be. Additional tracking data can also help to reduce the position uncertainty, particularly for a non-cooperative chaser object.

For the US Space Shuttle, a generalised analysis of TLE uncertainties has led to the definition of a shoe-box shaped volume, centred on the Shuttle position, with the following properties [31]:

- alert box: size  $\pm 5 \text{ km} \times \pm 25 \text{ km} \times \pm 5 \text{ km}$  (radial  $\times$  along-track  $\times$  out-of-plane); a conjunction predicted within the alert box causes increased sensor tasking, improved orbit determinations, and a switch to special perturbations methods (numerical integration of states)
- manoeuvre box: size  $\pm 2 \text{ km} \times \pm 5 \text{ km} \times \pm 2 \text{ km}$  (radial  $\times$  along-track  $\times$  out-of-plane); a conjunction predicted within the manoeuvre box causes the initiation of an avoidance manoeuvre, if the manoeuvre does not compromise either primary payload or mission objectives (NASA Flight Rule A4.1.3-6)

In the case of no avoidance manoeuvres, the mean probability of a collision between a catalog object of diameter  $d > 10 \text{ cm}$  and the Space Shuttle STS is on the order of 1 in 200,000 for a 10-day mission duration. The probability to encounter a mission critical damage from an untrackable object of 0.5 cm to 10 cm (or larger) in diameter is about two orders of magnitude higher, i.e. 1 in 2,000 per STS mission. Thus, more than 95% of the potentially mission critical impactors cannot be tracked by current operational surveillance systems. The most likely impact velocity on Space Shuttle for objects of  $d > 1 \text{ cm}$  is on the order of 9 km/s. ESA's ERS-1, ERS-2, and ENVISAT satellites have sun-synchronous, retrograde orbits of inclination 98.5 deg and mean altitude 780 km. In case of an impact by an object of  $d > 1 \text{ cm}$ , the mean collision velocity is on the order of 13 km/s (twice the kinetic energy as compared to STS). Due to higher object densities at ERS altitudes, the object flux also increases by a factor of about 10 with respect to STS altitudes. For a mean cross-section of  $30 \text{ m}^2$ , the probability of ERS-1 or ERS-2 being hit by a trackable object is on the order of 1 in 7,000 per year (or 1 in 250,000 in 10 days).

Six collision avoidance manoeuvres were performed by the US Space Shuttle during a total of 61 missions and 568 days on orbit (from STS-26 to STS-85). At four occasions (STS-48 in 1991, STS-53 in 1992, STS-72 in 1996, and STS-82 in 1997), a conjunction was predicted inside the Shuttle manoeuvre box ( $2 \text{ km} \times 5 \text{ km} \times 2 \text{ km}$ , extending along track). At two more occasions (STS-44 in 1991, and STS-57 in 1993), an avoidance manoeuvre was performed for a fly-by slightly outside the box, while in five cases (STS-27 in 1988, STS-61 in 1993, STS-71 in 1995, STS-79 in 1996, and

STS-82 in 1997) no avoidance was performed in spite of a conjunction within the STS manoeuvre envelope. The resulting mean avoidance manoeuvre frequency for Space Shuttle is on the order of 4 for each year on orbit, or 1 in 10 missions. If ESA's ERS satellites were operated according to NASA Flight Rule A4.1.3-6, with an accepted residual collision risk for trackable objects of 1 in 200,000 during a 10-day mission (or 1 in 5,500 for a year of on-orbit operation), then, on average, each ERS satellite would perform more than 80 avoidance manoeuvres per year (20 times the STS frequency). The Shuttle frequency can only be matched, if the dimensions of the ERS manoeuvre ellipsoid are downscaled by a factor of  $\approx 1/4$  (volume reduction by  $1/64$ ), with a corresponding accepted risk of collision of about 1 in 10,000 per conjunction event. Based on these criteria, the ERS-1 satellite performed a manoeuvre on 25-Jun-1997 and on 21-Mar-1998 to avoid a close conjunction with the Russian Kosmos-614 satellite, and with the US Hilat satellite, respectively. The French SPOT-2 satellite manoeuvred on 24-Jul-1997 to avoid an explosion fragment of a Thorad Agena D upper stage. Further manoeuvres for ERS and SPOT satellites could be avoided after improving TLE state vectors of the chaser objects with independent tracking data. If no avoidance manoeuvres would be performed, the mean time between collisions of ERS-type spacecraft with catalogue objects is on the order of 50 years.

If a conjunction of a trackable object with an operational spacecraft is predicted to exceed adopted threshold limits (e.g. in terms of predicted miss distance, or in terms of assessed collision probability), and if improved orbits based on tracking data of known accuracy confirm a high-risk conjunction, then an avoidance manoeuvre should be executed. Only in the case of marginal violations of the thresholds, the potential collision risk may be weighed against consequences on the mission operations and payload performance to determine if a manoeuvre should be performed. Depending on the notification and manoeuvre decision time prior to a conjunction event, mainly two different kinds of  $\Delta V$  efficient avoidance strategies can be envisaged:

- short-term strategy: increase the altitude separation distance at conjunction by means of a single  $\Delta V$  along-track manoeuvre of the target spacecraft  $n_{rev} + 1/2$  orbital revolutions prior to the event ( $n_{rev} = 0, 1, \dots$ )
- medium-term strategy: increase the along-track separation distance at conjunction by means of one or several small  $\Delta V$  along-track manoeuvres of the target spacecraft  $n_{rev}$  revolutions prior to the event (where  $n_{rev} \geq 2$  should be considered)

At ERS altitudes, the short-term avoidance strategy requires a  $\Delta V$  of about 0.3 m/s for each 1 km step increase in altitude separation, and it is best suited if notification times are short, or if the fly-by has a near head-on geometry, and if  $\Delta V$  (velocity change manoeuvre) requirements are not critical. This strategy was used for the two ERS-1 avoidance manoeuvres. The medium-term avoidance strategy for the same altitude regime requires a  $\Delta V$  of about  $0.06/n_{rev}$  (in m/s) for each 1 km step in along-track separation, where  $n_{rev} \geq 2$  is the number of coast orbits after the manoeuvre and before the conjunction. This strategy is best suited, if the notification time is sufficiently long, if the conjunction orbits are not co-planar, and if  $\Delta V$  budgets are critical. This concept was used for the SPOT-2 avoidance manoeuvre.

Due to the overcrowding of the GEO region, particularly in some preferred longitude sectors which are of interest for broadcasting and telecommunication, there is a tendency that more than one spacecraft gets allocated to the same longitude slot. Under international agreements such an assigned position has to be maintained within a deadband of  $\Delta\lambda = \pm 0.1$  deg, centred on the nominal longitude  $\lambda$ . In order to avoid close conjunctions between satellites in the same slot, coordinated measures of station keeping have to be introduced [32, 33]. Moreover, prior to its end of operational lifetime, each GEO satellite should be re-orbited to a graveyard orbit at least 300 km above the GEO ring, in order to avoid close conjunctions of dead objects with operational spacecraft.

## 1.11 Spacecraft protection

The effect of a hypervelocity impact on a spacecraft is, not surprisingly, dependent on impact energy. For the purposes of considering impact effects on a spacecraft design it is often useful to distinguish three debris size ranges:  $< 0.1$  mm,  $0.1$  mm –  $10$  mm, and  $> 10$  mm. A debris object smaller than  $0.1$  mm in size represents a very low penetration hazard to a spacecraft, but because the population of such objects is so large in LEO (several orders of magnitude greater than the trackable population), multiple impacts can occur. Over the mission life these impacts can cause an accumulation of minor damage to spacecraft surfaces, such as surface pitting and erosion. For debris in the  $0.1$  mm to  $10$  mm size range, significant structural damage can occur. This might include penetration of exposed instruments located on the outside of a spacecraft. Penetration of the structure and damage to internal equipment is another distinct possibility. Both effects could lead to partial or complete loss of a mission. It is generally considered unlikely that a spacecraft will survive an impact with a particle larger than  $\sim 10$  mm, mainly because of the penetrative damage caused. At the very least, the transfer of momentum may cause the spacecraft to lose attitude control. If the debris object is large enough, the post-impact stress waves could carry sufficient energy through the structure to cause a catastrophic break-up of a spacecraft. To further understand the damage effects on a spacecraft, the chapter examines the consequences of impacts on a selection of typical subsystems, such as solar panels, pressure vessels/tanks, steering/pointing mechanisms, electrical harness, and honeycomb panels.

Manned spacecraft debris protection can be enhanced by adding dedicated shielding. Typically, this is achieved by implementing a multiple wall shield. Such a shield is considered an efficient method of improving protection, and usually involves spacing one or more thin bumper layers in front of the spacecraft structure, or back-up wall. The effectiveness of a multiple wall shield is dependent on several factors, including impactor properties (mass, density, velocity, and shape), the material in each bumper, and the arrangement of the bumpers. Current shielding technology is limited to protecting against objects in LEO up to approximately  $1$  cm in diameter. The designs, materials and capabilities of some commonly considered shield types are given in the relevant Handbook chapter, including the Whipple shield, stuffed Whipple shield, multi-shock shield, and the mesh double-bumper shield.

The provision of additional shielding for unmanned spacecraft structures cannot rely on the techniques used for manned spacecraft, not least for reasons of mass, volume and cost. Instead, one is restricted to enhancing the design of honeycomb (HC) panels and/or MLI blankets. Therefore, it will not be possible to prevent  $1$  cm size LEO particles from penetrating; in fact a more achievable size limit is  $\sim 2$  mm. A number of shield options may be considered [34]. In particular, it was determined that a double-honeycomb design, as shown in Figure 1.11–1, could potentially reduce the number of penetrating particles by a factor of  $\sim 4$ , at an additional 'cost' of only  $1.2$  kg/m<sup>2</sup>, compared to a standard single-honeycomb panel. Double-honeycomb panels are particularly recommended for the most vulnerable spacecraft surfaces, e.g. those facing the velocity direction. Shielding approaches for solar array panels and pressure vessels are also given.

The characterisation of hypervelocity debris and meteoroid impacts on a spacecraft is an important element of its environmental risk analysis. Empirical damage equations are used to determine not only the size of an impact crater or hole on a spacecraft surface, but also the ballistic limit of a structure or shield. The ballistic limit is the critical size of particle that causes a structure or shield to fail. Failure can be defined in terms of penetration or spallation of the structure/shield. To date, two distinct types of ballistic limit equation have been derived to characterise the two possible types of spacecraft target design, namely single wall and multiple wall. The chapter provides a comprehensive review of available damage equations (crater and hole) and ballistic limit equations (single and multiple wall and honeycomb panel). Each equation is listed in parametric form with an accompanying table for specific parameter values found by different researchers for various target materials. Parameters include wall thickness, impactor diameter, impactor density, yield strength, impact velocity and angle, and wall spacing.

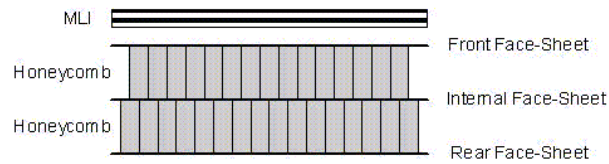


Figure 1.11-1: Double-Honeycomb Panel Structure with MLI

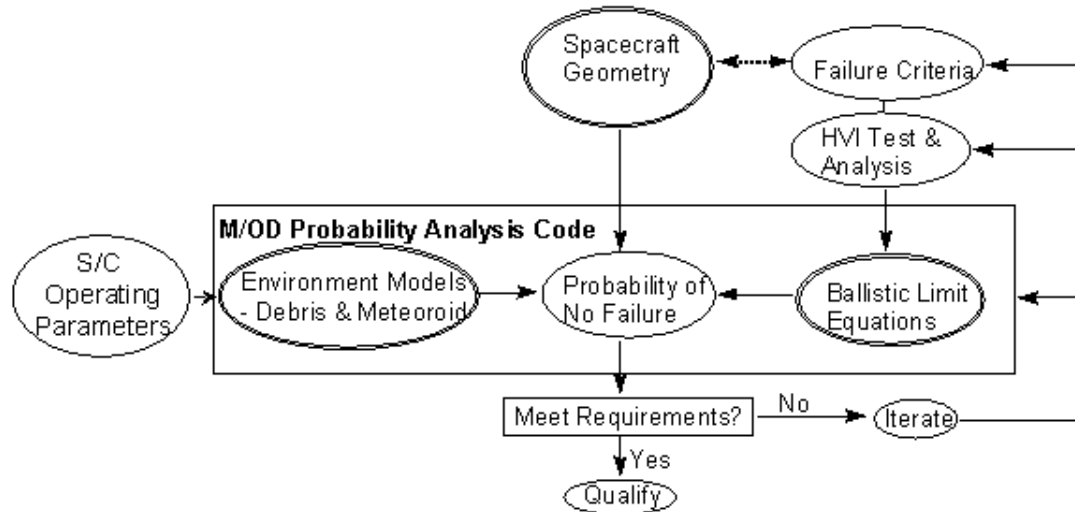


Figure 1.11-2: Standard impact risk assessment methodology for spacecraft

Finally, the chapter provides practical methodologies for assessing impact risk and implementing protection. Christiansen [35] has defined a standard impact risk assessment methodology for spacecraft, as shown in Figure 1.11-2 as an iterative process. A key aspect of this process is the utilisation of meteoroid/debris damage assessment tools. Several such models have been developed to provide reliable and accurate risk assessments. In general, the models can determine probability of penetration, the benefits of different shielding design options, or examine the effects of shadowing (where one part of a spacecraft provides protection to another). Three models currently used within Europe are ESA's ESABASE/DEBRIS, DLR's MDPANTO, and QinetiQ's SHIELD. These tools are compared in terms of their purpose and capabilities.

Spacecraft survivability can be greatly improved by relocating vulnerable components and placing sensitive equipment behind existing vehicle structures. It may even be possible for a spacecraft to survive an impact from a centimetre-size object through special consideration of the design (e.g. redundant subsystems, frangible structures, pressure vessel isolation, separation of redundant units, and routing of electrical cables, fluid lines, etc.) [36]. This is certainly the case for unmanned spacecraft, where the possibility of a degree of penetrative impact damage might be tolerable. General recommendations and guidelines for the design and placement of equipment to improve survivability are given in the chapter. For example: identify the areas of the satellite most vulnerable to debris impact (these are surfaces facing the velocity vector direction for most unmanned spacecraft in LEO circular polar orbits); identify mission-critical and sensitive equipment by performing a FMECA analysis (consideration of items such as batteries, propulsion tanks/pipes, reaction/momentum wheels and gyros is especially important); for internal equipment, move sensitive and critical units away from vulnerable surfaces (e.g. those facing the velocity vector) and/or place them behind (relative to the vulnerable face) less critical units or internal structure. The chapter concludes by providing actual examples of spacecraft protection implementation on the International Space Station and the unmanned Radarsat mission.

# 2

---

## THE HANDBOOK WEB ENVIRONMENT

## 2.0 The Handbook Web Environment

### Scope

Managing projects with internationally distributed study teams often raises certain problems concerning common management of documentation and source code. The goal of the Handbook Web Environment (HWE) was to provide a common platform for document and source code management for the study team. Furthermore, additional tools were developed to provide further services and information. This has been achieved by developing a web-based application written in Perl/CGI providing all information to the user without the need of any local installation.

In this context, the Handbook Web Environment was developed to

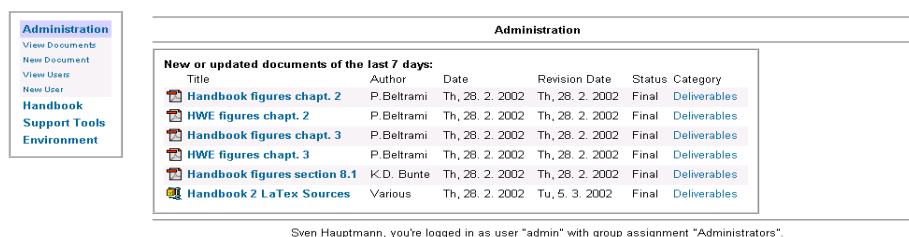
- Support project management and project control
- Provide a central platform for the development of documentation and software
- Visualize multi-dimensional data structures in addition to the handbook
- Simplify browsing through the handbook HTML version
- Provide printable copies for download in various formats

In order to achieve these goals, the handbook web environment has been divided into three separate branches: The Administrative Branch, The Document branch, and the Support Tool Branch.

### The Administrative Branch

The Administrative Branch covers the project management aspects of the HWE. It is only available to the project team during the project duration, providing personal password protected accounts for the study team members. Utilizing a group and user based permission system, all modules may be made available with different access rights to the users of the system. Personal information may be maintained by the users themselves or by the study management. The user database acts also as a project related contacts database for the study team members.

The core of the Administrative Branch is the document management system. It stores all relevant project documentation in various formats. The built-in revision control system keeps copies of all intermediate versions of a document in order to allow transparent editing and review processes between users.



The screenshot shows a web interface with a navigation menu on the left and a main content area. The navigation menu includes links for Administration, View Documents, New Document, View Users, New User, Handbook, Support Tools, and Environment. The main content area is titled 'Administration' and features a table of 'New or updated documents of the last 7 days'.

Title	Author	Date	Revision Date	Status	Category
Handbook figures chapt. 2	P. Beltrami	Th, 28. 2. 2002	Th, 28. 2. 2002	Final	<a href="#">Deliverables</a>
HWE figures chapt. 2	P. Beltrami	Th, 28. 2. 2002	Th, 28. 2. 2002	Final	<a href="#">Deliverables</a>
Handbook figures chapt. 3	P. Beltrami	Th, 28. 2. 2002	Th, 28. 2. 2002	Final	<a href="#">Deliverables</a>
HWE figures chapt. 3	P. Beltrami	Th, 28. 2. 2002	Th, 28. 2. 2002	Final	<a href="#">Deliverables</a>
Handbook figures section 8.1	K.D. Bunte	Th, 28. 2. 2002	Th, 28. 2. 2002	Final	<a href="#">Deliverables</a>
Handbook 2 LaTeX Sources	Various	Th, 28. 2. 2002	Tu, 5. 3. 2002	Final	<a href="#">Deliverables</a>

Below the table, a status message reads: 'Sven Hauptmann, you're logged in as user "admin" with group assignment "Administrators".'

Figure 2.0–1: Latest Additions and Updates

The screenshot displays a web interface for document management. On the left, there is a navigation menu with categories like 'Administration', 'View Documents', 'New Document', 'New User', 'Handbook', 'Support Tools', and 'Environment'. The main content area is titled 'View Documents' and shows a list of 'Available Categories' with columns for Name, Description, and Last Modified. Below this, there is a section for 'Available Documents in "Minutes:"' listing various documents like 'Minutes PM2', 'Handouts of the eta\_max Presentation at PM 2', 'PM1 Minutes', and 'KO Minutes' with their respective authors and dates.

Two callout boxes provide detailed information for the document 'Handouts of the eta\_max Presentation at PM 2':

**Document Details for "Handouts of the eta\_max Presentation at PM 2":**  
 Add a new revision  
 Document title: Handouts of the eta\_max Presentation at PM 2  
 Author(s): Pablo Beltrami, Sven Hauptmann  
 Description:  
 Document format: Adobe Portable Document Format (PDF)  
 URL:  
 Document name: R027\_PM2.pdf  
 Revision status: Final  
 Revision date: Thursday, 27. September 2001  
 Revision number: 1.0.0  
 Created at: Thursday, 27. September 2001  
 Created by: Sven Hauptmann

**Revision History for "Handouts of the eta\_max Presentation at PM 2"**

File	Revision number and status	Author	Reviewer	Created
R027_PM2-1.0.0.pdf	1.0.0, Final	Pablo Beltrami, Sven Hauptmann	Holger Sdunnus	Th, 27. 9. 2001/Sven Hauptmann

Comments:  
Final Version of the PM 2 Handouts

At the bottom of the page, a message reads: 'Sven Hauptmann, you're logged in as user "admin" with group assignment "Administrators".'

Figure 2.0–2: Document Details

## The Document Branch

Scope of the Document Branch is the management of the  $\text{\LaTeX}$  source code of the Space Debris Mitigation Handbook. During project duration, it is only available to the study team, providing a common codebase and revision history utilizing the Concurrent Versions System (CVS), a commonly known source control system (<http://www.cvshome.org>).

CVS, the Concurrent Versions System, is the dominant open-source network-transparent version control system. CVS is useful due to its following capabilities:

- Its client-server access method lets developers access the latest code from any Internet connection.
- Its unreserved check-out model to version control avoids artificial conflicts.
- Its client tools are available on most platforms.

The CVS may be accessed via the web interface (read-only) or via an external client (e. g. WinCVS, <http://www.wincvs.org>) for full interactive access of the repository.

Furthermore, a webbased service to convert the latest version of the handbook into various formats has been developed. This service converts the handbook into different formats for online viewing (HTML, PDF) or allows a download of printable copies (PDF, DVI, Postscript). The converted versions of the handbook will be made available to reviewers.

## The Support Tool Branch

The Handbook Support Tool branch provides a framework for an in-depth analysis of additional handbook figures. It is based on pre-processed information and provides linked HTML pages connecting each figure of the handbook with additional data. Additionally, an orbital lifetime calculator has been implemented for circular or near circular low-earth orbits.



**Administration**

**Handbook**

CVS-Tree

Conversion

Formats

**Support Tools**

Environment

**CVS-Tree**

---

Click on a directory to enter that directory. Click on a file to enter that file.

Current directory: [\[Root\]](#) / [R027](#)

File	Rev.	Age	Auth	Log
Previous Directory				
Chapters/				
HWE/				
Tables/				
figs/				
Handbook.bib	1.11	3 days	pablo	no message
Handbook2.tex	1.11	6 days	pablo	Added htmlonly path for the figures Minor corrections to chapt 2.5
Handbook2_pdf.tex	1.1	5 days	pablo	Handbook2.tex main file for creating the pdf version at the etamax server The
Handbook_etamax.bib	1.3	5 days	pablo	References corrected Figure 2.2-3 updated
Handbook_project.tcp	1.1	4 weeks	pablo	Handbok projectfile for TeXnicCenter added
array.sty	1.1	13 days	pablo	Latex classfiles and styles added
esahbook.cls	1.1	13 days	pablo	Latex classfiles and styles added
esahbook.lst	1.1	13 days	pablo	Latex classfiles and styles added
float.sty	1.1	13 days	pablo	Latex classfiles and styles added
handbook_driver.bat	1.2	6 days	pablo	Added htmlonly path for the figures Minor corrections to chapt 2.5
html.sty	1.1	13 days	pablo	Latex classfiles and styles added
longtable.sty	1.1	13 days	pablo	Latex classfiles and styles added
lscap.sty	1.1	13 days	pablo	Latex classfiles and styles added
rotate.sty	1.1	13 days	pablo	Latex classfiles and styles added

File	Rev.	Age	Author	Last log entry
Previous Directory				
Chapters/				
HWE/				
Tables/				
figs/				

Show only files with tag:

Sven Hauptmann, you're logged in as user "admin" with group assignment "Administrators".

Figure 2.0-3: Viewing files in CVS repository

**Administration**

**Handbook**

CVS-Tree

**Conversion**

Formats

**Support Tools**

Environment

**Conversion**

---

File	Last conversion date	Size (MB)
<a href="#">zipped DVI version</a>	Tue Mar 5 11:16:33 2002	4.8
<a href="#">Postscript version</a>	Tue Mar 5 11:17:42 2002	38.2
<a href="#">PDF version</a>	Tue Mar 5 11:24:46 2002	6.8
<a href="#">HTML version</a>	Tue Mar 5 11:49:51 2002	10.8

---

Sven Hauptmann, you're logged in as user "admin" with group assignment "Administrators".

Figure 2.0-4: Format Conversion

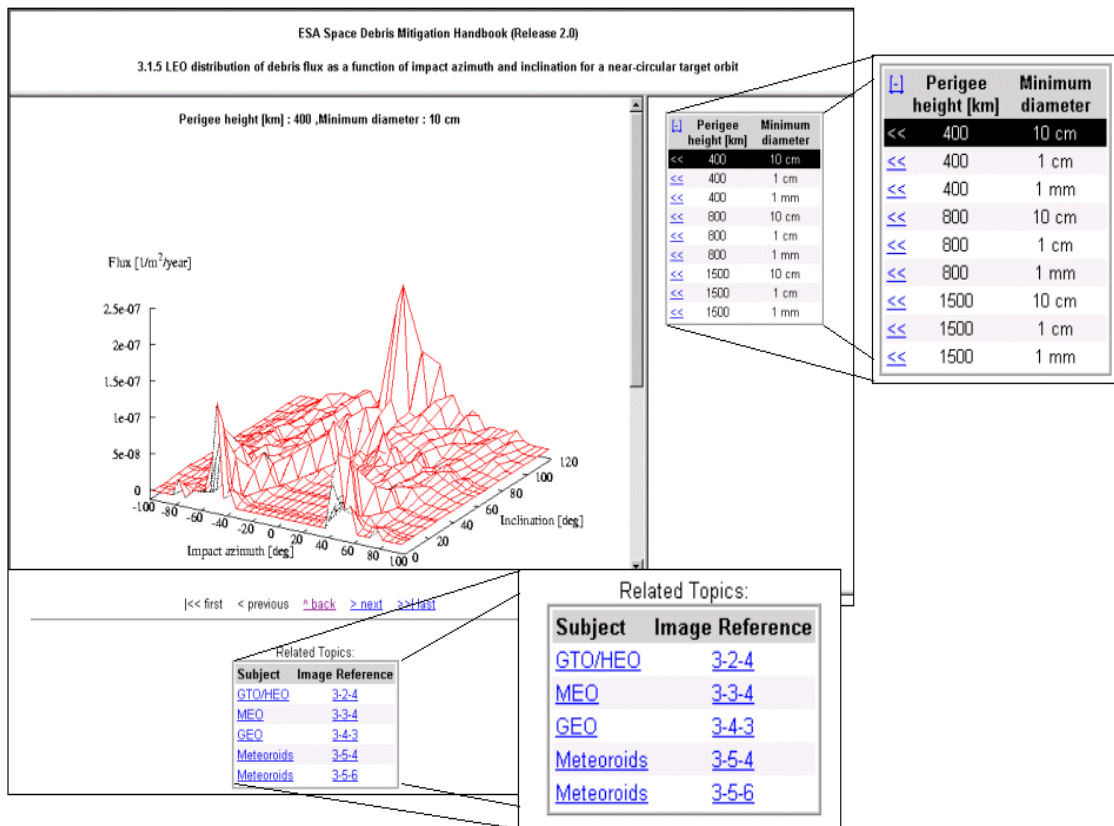


Figure 2.0–5: Support Tools Figure Display

Administration

Handbook

**Support Tools**

Orbital lifetime calculation

List of Figures

generate Figures

Environment

### Orbital lifetime calculation

Solar Activity	<input type="text" value="Medium"/>	
Perigee Height	<input type="text" value="400.0041"/>	[200 < hp < 800 (km)]
Eccentricity	<input type="text" value="0.0000"/>	[.0000 < e < .0500]
Orbital Inclination	<input type="text" value="51.0000"/>	[5 < i < 51 (deg)]
Mass to Area ratio	<input type="text" value="20"/>	[>=10(kg/m²)]
<b>Orbital Lifetime</b>	<b>0.10404</b>	[yr]

This tool calculates the expected orbital lifetimes for an object with a specified mass-to-area ratio and the given orbital parameters. The results are taken from a table of pre-calculated values. The results will not be interpolated between data points. Therefore, the input parameter may be subject to a change during calculation. After calculation, used values will be shown in the input fields of the form.

---

Sven Hauptmann, you're logged in as user "admin" with group assignment "Administrators".

Figure 2.0–6: Orbital Lifetime Calculator

3

---

CONCLUSIONS

### 3.0 Summary and Conclusions

The ESA Space Debris Mitigation Handbook Second Edition was jointly produced in 2002 by an industrial consortium (QinetiQ and eta\_max space) and ESA/ESOC, under an ESA contract. The Handbook is a non-regulatory, self-standing document, providing technical information in support of European debris mitigation standards. The necessity of debris mitigation is illustrated in the context of historic launch activities and operational practices, which led to the current debris environment, with corresponding collision flux levels. Based on detailed population evolution models, this initial population is analysed with respect to its growth and stability under different traffic assumptions. The implementation of debris mitigation measures, in particular the de-orbiting of spacecraft and upper stages, is shown to reduce the debris growth to an acceptable level within a few decades. The risk on ground due to re-entering space objects, its assessment, and its control is also analysed. For on-orbit systems, collision risk reduction by avoidance manoeuvres, and passive protection by shielding is outlined. ESA's Handbook also compares recommended debris mitigation and risk reduction practices proposed by several other space agencies. The Handbook will be available by the end of 2002 following a lengthy review and approval process.

# Glossary

CVS	Concurrent Version System
DELTA	Debris Environment Long Term Analysis
DISCOS	Database and Information System Characterising Objects in Space
EOL	End Of Life
EURECA	European Retrievable Carrier
FMECA	Failure Modes Effects and Criticality Analysis
GEO	Geostationary Earth Orbit
GLONASS	Global Navigation Satellite System
GTO	Geostationary Transfer Orbit
GPS	Global Positioning System
HEO	Highly Eccentric Orbit
HST	Hubble Space Telescope
KSC	Kennedy Space Center
LEO	Low Earth Orbit
MASTER	Meteoroid and Space Debris Terrestrial Environment Reference
MEO	Medium Earth Orbit
MLI	Multi Layer Insulation
NPS	Nuclear Power Source
RTG	Radioactive Thermoelectric Generator
SRM	Solid Rocket Motor
SCARAB	SpaceCraft Atmospheric Reentry and Aerothermal Breakup
TLE	Two Line Elements

# BIBLIOGRAPHY

---

- [1] F. Pina Caballero, B. Fernández Montoto, and H. Klinkrad. DISCOS space data publication and documentation system. In *Proceedings of the 3rd European Conference on Space Debris (ESA SP-473)*, pages 795–799, ESOC, Darmstadt, Germany, 2001.
- [2] H. Klinkrad, J. Bendisch, H. Sdunnus, P. Wegener, and R. Westerkamp. An introduction to the 1997 ESA MASTER model. In *Proceedings of the 2nd European Conference on Space Debris (ESA SP-393)*, ESOC, Darmstadt, Germany, 1997.
- [3] H. Sdunnus, J. Bendisch, and H. Klinkrad. The ESA MASTER'99 space debris and meteoroid reference model. In *Proceedings of the 3rd European Conference on Space Debris (ESA SP-473)*, pages 299–307, ESOC, Darmstadt, Germany, 2001.
- [4] N. Johnson, P. Anz-Meador, E. Cizek, and S. Portman. History of on-orbit satellite fragmentations. 12th edition, NASA/JSC JSC29517, July 2001.
- [5] H. Klinkrad, J. Bendisch, K.D. Bunte, H. Krag, H. Sdunnus, and P. Wegener. The MASTER-99 space debris and meteoroid environment model. In *COSPAR 2000 Conference*, July 2000.
- [6] K.D. Bunte. Populations for a Divine based space debris model. In *Proceedings of the 3rd European Conference on Space Debris (ESA SP-473)*, pages 279–285, ESOC, Darmstadt, Germany, 2001.
- [7] B. J. Anderson and R. E. Smith. *Natural Orbital Environment Guidelines for Use in Aerospace Vehicle Development*. NASA TM 4527, June 1994. Chap. 7.
- [8] D. J. Kessler. Collision cascading: The limits of population growth in low earth orbit. *Advances in Space Research*, 11(12):63–66, 1991.
- [9] P. Eichler and D. Rex. Debris chain reactions AIAA-90-1365. *AIAA/NASA/DOD Orbital Debris Conference: Technical Issues & Future Directions*, Baltimore MD, USA, April 1990.
- [10] P. Krisko. EVOLVE 4.0 sensitivity study results. *Orbital Debris Quarterly News, Orbital Debris Program Office, NASA Johnson Space Center, Vol. 5, Issue 1*, January 2000.
- [11] L. Anselmo, A. Rossi, and C. Pardini. Updated results on the long-term evolution of the space debris environment. *Advances in Space Research*, 23(1):201–211, 1999.
- [12] H. Klinkrad, editor. *ESA Space Debris Mitigation Handbook*. European Space Agency, first edition, April 1999.
- [13] R. A. Madler and R. D. Culp. The impact of satellite breakup parameters on long-term orbital debris environment evolution. *SPIE Vol. 2483*, pp. 64–76, 1995.
- [14] N. L. Johnson, P. H. Krisko, J.-C. Liou, and P. D. Anz-Meador. NASA's new breakup model of EVOLVE 4.0. *33rd COSPAR Scientific Assembly, Warsaw, Poland*, July 2000.

- [15] *NASA Safety Standard: Guidelines and Assessment Procedures for Limiting Orbital Debris*, NSS 1740.14 edition, August 1995.
- [16] *CNES Exigence de Securite — Debris Spatiaux: Methode et Procedure*, MPM-51-00-12, issue 1 - revision 0 edition, April 1999. French version.
- [17] European space debris safety and mitigation standard (DRAFT), issue 1, revision 3, November 2001.
- [18] *NASDA Space Debris Mitigation Standard*, NASDA-STD-18 edition. Original Issue: 28 March 1996.
- [19] *Russian Aviation & Space Agency (RASA) Branch Standard — General Requirements for Mitigation of Space Debris Population*. Date of enforcement: 1st July 2000.
- [20] *US Government Orbital Debris Mitigation Standard Practices*, December 1997.
- [21] A. Kato. Comparison of mitigation standards and future co-operation work, B0.1-PE-0031. 33<sup>rd</sup> COSPAR Scientific Assembly, Warsaw (Poland), 2000.
- [22] J. P. Loftus and A. Kato. The status of mitigation standards and practices, IAA-00-IAA.6.6.09. 51<sup>st</sup> IAF, Rio de Janeiro, Brazil, October 2000.
- [23] S.A. Bouslog, B.P. Ross, and C.B. Madden. Space debris re-entry risk analysis. In *AIAA 94-0591, 32nd Aerospace Sciences Meeting*, Reno, USA, Jan 1994.
- [24] G. Koppenwallner et al. Spacecraft disintegration during atmospheric re-entry. Final report of ESOC contract 11427/95/D/IM, 1997.
- [25] H. Klinkrad, B. Fritsche, and A. Kashkovsky. Prediction of spacecraft destruction during uncontrolled re-entries. In *Proceedings of the European Conference on Spacecraft Structures, Materials and Mechanical Testing (ESA SP-468, Mar 2001)*, ESTEC, Noordwijk, The Netherlands, Nov 2000.
- [26] G. Koppenwallner, B. Fritsche, and T. Lips. Survivability and ground risk potential of screws and bolts of disintegrating spacecraft during uncontrolled re-entries. In *3rd European Conference on Space Debris*, ESOC, Darmstadt, Germany, Mar 2001.
- [27] *NASA safety standard: Guidelines and assessment procedures for limiting orbital debris*. NSS 1740.14, August 1995.
- [28] R. O'Hara, M. Matney, M. Jansen, and P. Anz-Meador. Latest revisions to the NASA debris assessment software (DAS). In *IAA-01-IAA.6.6.06, 52nd IAF-Congress*, Toulouse, France, Oct 2001.
- [29] N.L. Johnson and D.S. McKnight. *Artificial Space Debris*. 2nd edition. Orbit Book Comp., 1991. 0-89464-043-7.
- [30] UNCOPUOS. Principles relevant to the use of nuclear power sources in outer space. general assembly, 47th session, supplement no.20, A/47/20, 1992.
- [31] Committee on ISS Meteoroid/Debris Risk Management. *Protecting the Space Shuttle from Meteoroids and Orbital Debris*. National Research Council (NRC), 1997.
- [32] E.M. Soop. *Handbook of Geostationary Orbits*. Space Technology Library. Microcosm, 1994. ISBN 0-7923-3054-4.
- [33] A. Tanaka, H. Mineno, and M. Miyashita. Station keeping methods for two broadcasting satellites in the same geostationary position. In *Proc. of the 2nd International Symposium on Spacecraft Flight Dynamics*, ESA SP-255, page 141 ff, Darmstadt, 1986.
- [34] R. Turner et al. Cost-effective debris shields for unmanned spacecraft: Final report, issue 1. Submitted to ESA under Contract No. 12378/97/NL, December 1999.

- [35] E. L. Christiansen. NASA progress report. *Protection Working Group meeting, 16<sup>th</sup> IADC, Toulouse, France, November 1998.*
- [36] Scientific and Technical Subcommittee of UNCOPUOS. Technical report on space debris, A/AC.105/720, May 1999.